DOI: 10.1002/cbic.201100104

Ribosomal Synthesis of Backbone-Macrocyclic Peptides Containing γ-Amino Acids

Yukinori Ohshiro,[b] Eiji Nakajima,[c] Yuki Goto,[a] Shinichiro Fuse,[d] Takashi Takahashi,[d] Takayuki Doi,[e] and Hiroaki Suga*[a, b, c, f]

Pepstatin, discovered in 1970 as an extraordinarily potent inhibitor of pepsin, is a classical example of a γ-amino acid-containing natural product.[1] It has been proven that the statine residue, (3*S*,4*S*)-4-amino-3-hydroxy-6-methylheptanoic acid, mimics the tetrahedral transition-state structure of peptide-bond hydrolysis.[2] This knowledge led to the development of specific inhibitors of clinically relevant aspartic proteases, including renin and HIV proteases.[3] More recently, a new class of γ-amino acid-containing natural products has been discovered that is active against a non-protease enzyme. Spiruchostatin A, which was isolated from *Pseudomonas* sp., is a representative example; it has a macrocyclic structure containing a D-valine-derived (3*S*,4*R*)-statine and acts as a histone deacetylase inhibitor.[4] Clearly, the statine residue in this molecule does not act as a transition-state analogue but rather serves as a critical component of the macrocyclic scaffold. Moreover, didemnins B, isolated from the genus *Tridemnum* as an agent against kidney and epithelial ovarian cancer, has a γ-amino acid, isostatine, and also has a macrocyclic moiety.[5] These examples imply that statine and probably other γ-amino acids in a macrocyclic scaffold can be versatile structural elements for constructing bioactive peptides. Despite the attractiveness of γ-amino acid-containing peptides, their availability still relies on the traditional methodologies, that is, the serendipitous discovery of bioactive γ-amino acid-containing peptides from secondary-metabolite sources or by chemical synthesis from small libraries. We here report a new methodology involving genetic code reprogramming to ribosomally express backbone-cyclized peptides containing γ-amino acids (Figure 1 A) that potentially gives us more diverse libraries of γ-amino acid-containing peptides with a greater ease.

Since the translation apparatus allows for the facile construction of a peptide library with vast diversity, ribosomal synthesis of drug-like peptides can be a powerful tool for discovering novel bioactive compounds.[6] However, despite a number of reports describing the incorporation of various nonstandard amino acids into nascent peptide chains by using a conventional strategy such as nonsense or frame-shift suppression,[7] to the best of our knowledge, a successful demonstration of ribosomal incorporation of γ-amino acids has never appeared in literature. There are two reasons for this failure: 1) γ-Aminoacyl-tRNA is not stable under near-neutral aqueous conditions as the γ-amino group tends to intramolecularly attack the acyl group on the 3′ terminus of tRNA; this results in self-deacylation. 2) Even if some fractions of γ-aminoacyl-tRNA can be brought into the ribosome A site, the ribosome very likely fails to promote the peptidyl-transfer reaction as its catalytic environment is incompatible with bond formation between the γ-amino group and the acyl group on the P site tRNA.[8] As a result, no successful example of expressing any peptide containing γ-amino acids has been reported.

We have recently developed two new methods of generating unique peptides by using a custom-made, reconstituted, cell-free translation system integrated with flexizymes (flexible tRNA aminoacylation ribozymes)[9] and referred to as FIT (flexible in-vitro translation) system.[10] Using this system, we reprogrammed an initiation event in translation in which a FIT system lacking methionine was supplemented with a $tRNA^{fMet}_{CAU}$ charged with short exotic peptides by flexizyme; thereby, peptides containing unusual auxiliary residues at the N terminus were expressed.[11] The second method was ribosomal synthesis of backbone-cyclic peptides in a FIT system in which a codon was assigned to glycolic acid (^{HO}G). Expression of linear peptides bearing cystidyl-prolidyl-glycolate (C-P-^{HO}G) resulted in self-rearrangement[12] into peptides with a C-terminal diketopiperadine (dkp) thioester upon cleavage of the ester bond between P and ^{HO}G. The presence of two recombinant enzymes, peptide deformylase (PDF) and methionine aminopeptidase (MAP), in the FIT system generates an N-terminal free amino group that spontaneously reacts with the intramolecular dkp-thioester to afford the backbone-cyclized peptides.[13]

Although direct acylation of γ-amino acid onto tRNA would suffer from self-deacylation through intramolecular cyclization, acylation of a dipeptide consisting of γ- and α-amino acids onto tRNA could avoid such an undesired side reaction. To test whether this approach would yield stable peptidyl-tRNAs, we

[a] *Dr. Y. Goto, Prof. Dr. H. Suga*
Department of Chemistry, Graduate School of Science
The University of Tokyo
7-3-1, Hongo, Bunkyo, Tokyo 113-0033 (Japan)
Fax: (+81) 3-5841-8372
E-mail: hsuga@chem.s.u-tokyo.ac.jp

[b] *Y. Ohshiro, Prof. Dr. H. Suga*
Department of Advanced Interdisciplinary Studies
Graduate School of Engineering, The University of Tokyo
4-6-1, Komaba, Meguro, Tokyo 153-8904 (Japan)

[c] *Dr. E. Nakajima, Prof. Dr. H. Suga*
Department of Chemistry and Biotechnology
Graduate School of Engineering, The University of Tokyo
7-3-1, Hongo, Bunkyo, Tokyo 113-8656 (Japan)

[d] *Dr. S. Fuse, Prof. Dr. T. Takahashi*
Department of Applied Chemistry, Tokyo Institute of Technology
2-12-1, Ookayama, Meguro, Tokyo 152-8552 (Japan)

[e] *Prof. Dr. T. Doi*
Graduate School of Pharmaceutical Sciences, Tohoku University
6-3, Aza-aoba, Aramaki, Aoba, Sendai, Miyagi 980-8578 (Japan)

[f] *Prof. Dr. H. Suga*
WCU Department of Molecular Medicine and Biopharmaceutical Sciences
Seoul National University, Seoul 151-742 (Korea)

Supporting information for this article is available on the WWW under http://dx.doi.org/10.1002/cbic.201100104.

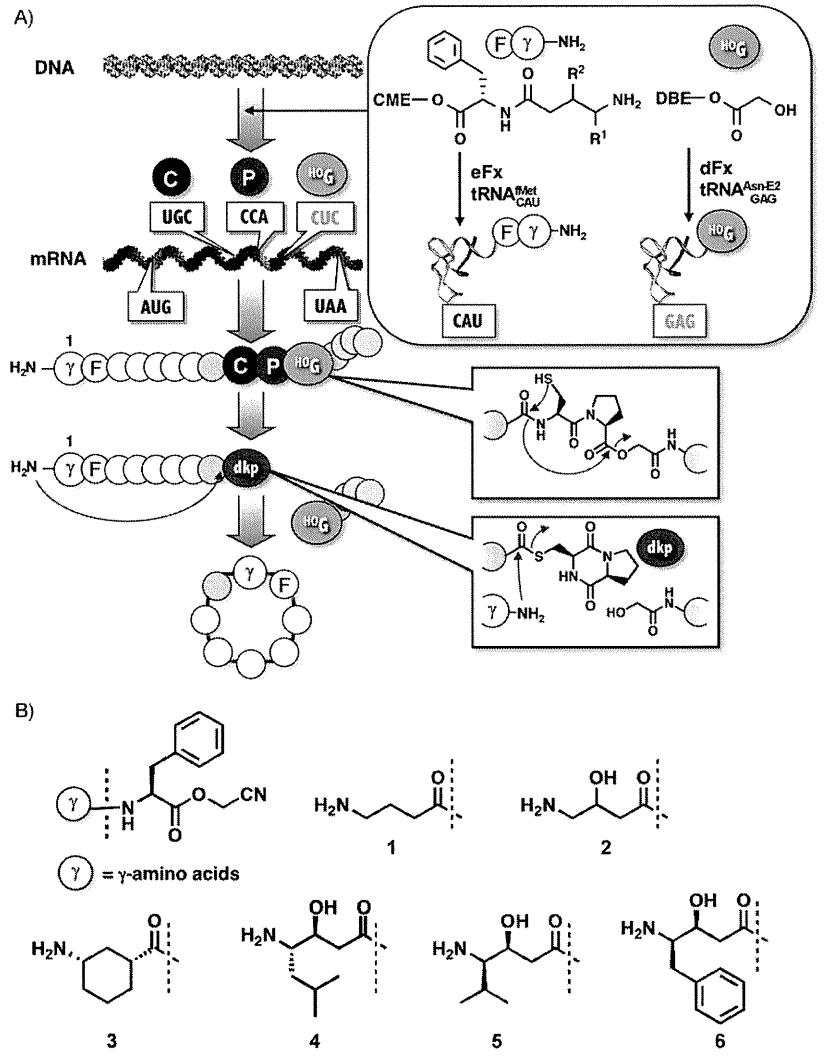

Figure 1. A) Outline of the ribosomal synthesis of cyclic γ-peptides. A linear precursor peptide containing a γ-amino acid at the N terminus and a C-P-^{HO}G motif downstream is expressed in a FIT system that lacks M and L and supplied with γ-aa-F-tRNA$^{fMet}_{CAU}$ and ^{HO}G-tRNA$^{AsnE2}_{GAG}$. Self-rearrangement of the C-P-^{HO}G segment to form dkp-thioester and the subsequent intramolecular addition of the N-terminal γ-amino group to the C-terminal thioester results in a backbone-cyclized peptide containing the γ-amino acid. B) γ-aa-F-CMEs used in this study. Each γ-amino acid (**1**: 4-aminobutyric acid, **2**: (*R*/*S*)-4-amino-3-hydroxy butyric acid, **3**: (3-aminocyclohexane)carboxylic acid, **4**: (3*S*,4*S*)-4-amino-3-hydroxy-6-methylheptanoic acid, **5**: (3*S*,4*R*)-4-amino-3-hydroxy-5-methylhexanoic acid, **6**: (3*S*,4*R*)-4-amino-3-hydroxy-5-phenylpentanoic acid) is chemically coupled with F-CME to obtain the corresponding dipeptide, and its tRNA aminoacylation is performed with flexizyme.

chose six γ-amino acids, including 4-aminobutanoic acid, statine, and its analogues, and condensed them with phenylalanine cyanomethyl ester (F-CME) to generate the corresponding γ-amino-dipeptide-CMEs **1**–**6** (Figure 1B). All the γ-amino-dipeptides were charged onto the acceptor analogue of tRNA, microhelix RNA, by a flexizyme (eFx), and the resulting γ-amino-dipeptidyl-RNAs were confirmed by acid-PAGE (Figure S1 in the Supporting Information). Moreover, when a model mRNA is expressed in a methionine-deficient FIT system containing γ-amino-dipeptide-tRNA$^{fMet}_{CAU}$ (Figure S2A), the γ-amino-dipeptides were successfully assigned as a reprogrammed initiator; this indicated that the designated model peptides bearing N-terminal γ-amino acids were generated with satisfactorily high expression profiles (Figure S2B) as well as the correct molecular mass (determined by MALDI-TOF MS; Figure S2C). These results clearly demonstrated that reprogramming the initiation event with short peptides containing γ-amino acids is a versatile and efficient method of ribosomally expressing polypeptides bearing γ-amino acids at the N terminus.

Having successfully incorporated γ-amino acids into the expressed peptides, we envisioned that this γ-amino-dipeptide initiation approach could be integrated with C-terminal dkp-thioester formation to promote the head-to-tail backbone cyclization (Figure 1A). Because no terminus in the final cyclic peptide is generated in this strategy, the γ-amino acid is embedded in the middle of sequence, that is, a defect of the γ-amino-dipeptide initiation approach, in which the position of the γ-amino acid is limited to the N terminus, can be overcome. We first designed an mRNA with the AUG initiation and CUC leucine elongation codons reprogrammed with γ-amino-dipeptides and ^{HO}G, respectively, to synthesize a model cyclic peptide containing a γ-amino acid (Figure 2A). With the above reprogrammed genetic code supported by a FIT system lacking M and L and supplied with **1**-F-tRNA$^{fMet}_{CAU}$ and ^{HO}G-tRNA$^{AsnE2}_{GAG}$, the peptide bearing γ-amino acid **1** at the N terminus and a C-P-^{HO}G segment in the downstream region was synthesized. After incubation at 37 °C for 12 h to facilitate the self-rearrangement of C-P-^{HO}G to dkp-thioester and subsequent macrocyclization, the peak corresponding to the expected backbone-cyclic peptide (**7**–**1**, Figure 2B) along with a minor peak with the molecular weight of a linear peptide generated by hydrolysis of the thioester intermediate (**8**–**1**, Figure 2C) was detected in the MALDI-TOF mass spectrum (Figure 2D). Tandem mass spectrometry of **7**–**1** proved the formation of an amide bond between the N-terminal γ-amino acid and the glycine at the ninth position (Fig-

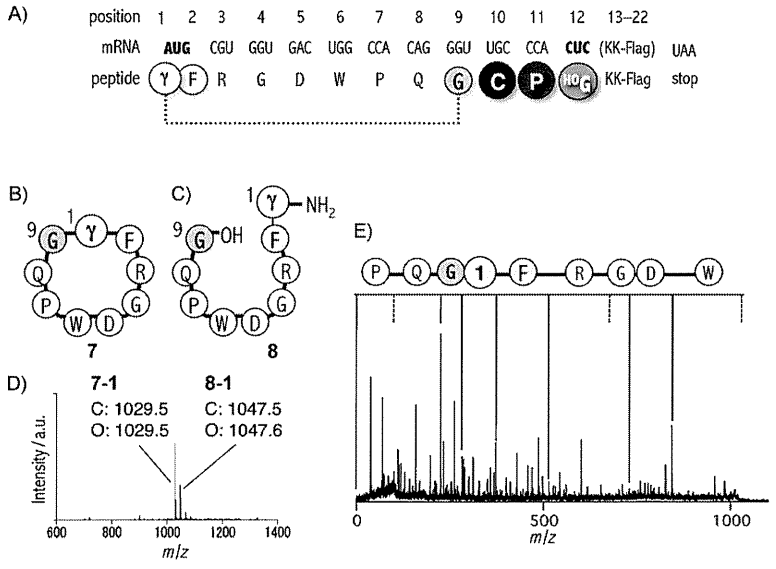

Figure 2. Ribosomal synthesis of backbone-cyclic peptides containing γ-amino acids by thioesterification. A) Sequences of the mRNA and the expressed linear precursor peptide. AUG and CUC codons are reassigned with γ-aa-F (γ-aa = **1**–**6**) and ^{HO}G, respectively. The KK-Flag in parenthesis indicates the RNA sequence encoding this peptide (KK-DYKDDDDK). The dotted line shows the ring-closing pattern after macrocyclization. B) Schematic structure of the objective γ-amino acid-containing cyclic peptide (**7**). "γ" indicates various γ-amino acid residues (**1**–**6**). The residue numbering is given. C) Schematic structure of the linear hydrolysate of the dkp-thioester intermediate (**8**). D) Mass spectrum of the reaction product from reprogrammed translation with **1**-F initiator. The detected peaks corresponding to the cyclic product (**7**–**1**) and hydrolysis product (**8**–**1**) were labeled in the spectrum. The calculated mass (C) and observed mass (O) for singly charged species, $[M+H]^+$, are also shown in the spectrum. E) Tandem mass spectrum of **1** containing cyclic peptide (**7**–**1**). Peaks corresponding to a set of assigned sequential fragment ions, generated by cleavage of two amide bonds, are shown.

ure 2E). These data demonstrate ribosomal synthesis of backbone-cyclic peptide containing a γ-amino acid. When we used dipeptides bearing relatively small γ-amino acids (**1** and **2**) as reprogrammed initiators, the objective macrocyclic peptides were generated as the main products (Figure S3A); however, in the case of more sterically demanding γ-amino acids (**3**–**6**), a peak corresponding to the linear peptide in which the peptide bond between G9 and C10 was cleaved (originating from the hydrolysis of dkp-thioester) dominated the mass spectra (Figure S3B–E); in particular when **5**- or **6**-F-tRNA$^{fMet}_{CAU}$ was used, no desired backbone-macrocyclic peptide was observed. This was a serious limitation of the present strategy.

To increase the level of production of backbone macrocyclization, we embedded cysteine residues in the peptide sequence (Figure 3A). We expected that their sulfhydryl side chains could rapidly form cyclic thioester intermediates by intramolecular trans-thioesterification, thereby promoting the subsequent attack of N-terminal γ-amino group on the thioester, possibly with a decreased level of the competing hydrolysis (Figure S4). An mRNA (Figure 3C) was designed based on a scaffold of bicyclic sunflower trypsin inhibitor-1 (SFTI-1)[14] and expressed under the same reprogrammed genetic code in the presence of various γ-amino-dipeptidyl-tRNA$^{fMet}_{CAU}$. The resulting translation product was incubated for 16 h to promote backbone macrocyclization in situ. In all cases, we observed a peak corresponding the desired backbone-macrocyclic peptide **9**, but the level of competing hydrolysis product **10** depended on the γ-amino acids (Figure 3D). It should be noted, however, that the consistent observation of the backbone-macrocyclic peptides throughout the γ-amino acid kinds indicates the reliability of this strategy.

In summary, we have developed a method to express peptides bearing γ-amino acid at the N terminus by reprogramming the genetic code of initiation using various dipeptide initiators. To the best of our knowledge, this is the first demonstration of ribosomal synthesis of γ-amino acid-containing polypeptides. Moreover, this methodology was coupled with the in situ generation of dkp-thioester at the C terminus of the peptide to yield backbone-macrocyclic peptides containing various γ-amino acids at an internal position. Given the previous report that the reprogrammed initiation event accepts short peptides of a wide variety of nonstandard structures, such as D-, β-, *N*-methyl, and α-disubstituted amino acids, as well as aminobenzoic acids,[11c] this methodology should be applicable to the ribosomal synthesis of backbone-macrocyclic peptides containing diverse nonstandard amino acids, thereby enabling us to construct exotic macrocyclic peptide libraries and explore new chemical space for novel functions.

Experimental Section

Flexizyme acyl-tRNAs were prepared by aminoacylation according to the following procedure. For γ-aa-F-tRNA$^{fMet}_{CAU}$, tRNA$^{fMet}_{CAU}$ (6.25 μL, 40 μM) in Tris-HCl (0.1 M, pH 8.0) was heated at 95 °C for 1 min, then cooled to room temperature over 5 min. $MgCl_2$ (2.5 μL, 3 M) and eFx (1.25 μL, 200 μM) were added to the solution, which was incubated at room temperature for 5 min. γ-aa-F-CMEs in DMSO (2.5 μL, 25 mM each) were then added to the mixture, which was incubated on ice for 2 h. ^{HO}G-tRNA$^{AsnE2}_{GAG}$ was synthesized as previously reported.[13] Each acylation reaction was quenched by the addition of sodium acetate (40 μL, 0.6 M, pH 5.0), and the acyl-tRNA was recovered by ethanol precipitation. The pellet was rinsed twice with 70% ethanol with sodium acetate (0.1 M, pH 5.0) and once with 70% ethanol, then dried and stored at −80 °C. The acyl-tRNAs were dissolved in sodium acetate (0.5 μL, 1 mM) just before being added to the translation mixture.

For reprogrammed translation initiation with γ-amino acids, translation mixture was prepared as previously reported.[10,11c,13] Translation was carried out in a reaction mixture containing Thr, Tyr, Lys,

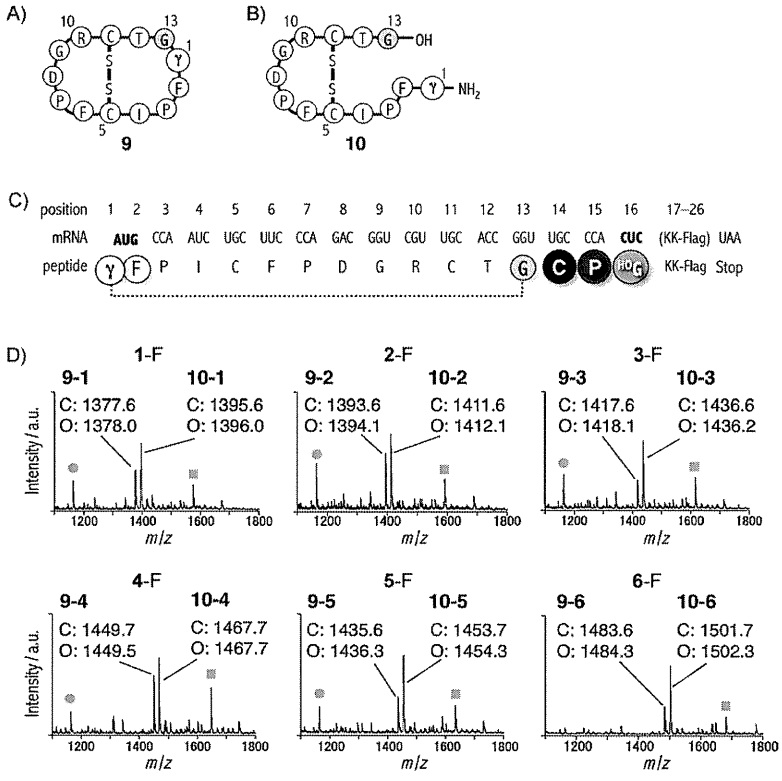

Figure 3. Ribosomal synthesis of bicyclic peptides containing γ-amino acids by thioesterification. A) Schematic structure of the bicyclic peptides closed by a backbone peptide bond and a disulfide bond (**9**). "γ" indicates various γ-amino acid residues (**1**–**6**). Residue numbering is shown. B) Schematic structure of the hydrolysate of dkp-thioester intermediate (**10**). C) Sequences of the mRNA and the expressed linear precursor peptide. AUG and CUC codons are reassigned with γ-aa-F (γ-aa = **1**–**6**) and ^{HO}G, respectively. The KK-Flag in parenthesis indicates the RNA sequence encoding this peptide (KK-DYKDDDDK). The dotted line shows the ring-closing pattern after macrocyclization. D) Mass spectra of the reaction product from reprogrammed translation with γ-aa-F dipeptide initiators. The detected peaks corresponding to the cyclic product (**9**-γ-aa) and hydrolysis product (**10**-γ-aa) are labeled in the spectra (γ-aa = **1**–**6**). The calculated (C) and observed (O) masses of singly charged species, $[M+H]^+$, are also shown in the spectra. The peaks corresponding to a translation side product initiated with Pro at the third position and a side product generated by addition of a cysteine onto the thioester intermediate are shown by gray circles and squares, respectively.

and Asp (200 μM each), various γaa-F-tRNA$^{fMet}_{CAU}$ molecules (50 μM) and DNA template1 (40 nM). The translation mixture (5 μL total volume) was incubated at 37 °C for 1 h. The resulting translation product was analyzed by Tricine-SDS PAGE or MALDI-TOF MS in a previously reported manner.[9–11]

For the ribosomal synthesis of cyclic peptides containing γ-amino acids, translation was carried out in a reaction mixture containing minimum required amino acids (200 μM each), γ-aa-F-tRNA$^{fMet}_{CAU}$ (100 μM), ^{HO}G-tRNA$^{AsnE2}_{GAG}$ (100 μM), and DNA template2 (40 nM). The mixture (10 μL) was incubated at 37 °C for 16 h to facilitate the translation reaction and macrocyclization. The reaction was quenched by adding 1% TFA (10 μL). The product was desalted on a C18 SPE column (T300-C18, Nikkyo Technos) and eluted with 80% acetonitrile/0.5% acetic acid (1.2 μL) saturated with (*R*)-cyano-4-hydroxycinnamic acid. The mass was measured by MALDI-TOF MS (autoflex TOF/TOF, Bruker) using the linear mode and externally calibrated with peptide calibration standard II (Bruker). Tandem mass spectrometry was also performed by using autoflex TOF/TOF in the lift mode.

Acknowledgements

This work was supported by grants from the Japan Society for the Promotion of Science Grants-in-Aid for Specially Promoted Research (21000005), and a research and development projects from the Industrial Science and Technology Program in the New Energy and Industrial Technology Development Organization (NEDO) to H.S., grants from the Japan Society for the Promotion of Science Grants-in-Aid for Young Scientists (B) (22750145) to Y.G., and the Global COE Program "Chemistry Innovation through Cooperation of Science and Engineering", MEXT, Japan to E.N.

Keywords: amino acids · genetic code reprogramming · macrocycles · peptides · ribosomal synthesis · statines

[1] H. Umezawa, T. Aoyagi, H. Morishima, M. Matsuzaki, M. Hamada, *J. Antibiot.* **1970**, *23*, 259.

[2] a) H. Morishima, T. Takita, T. Aoyagi, T. Takeuchi, H. Umezawa, *J. Antibiot.* **1970**, *23*, 263; b) N. Marks, A. Grynbaum, A. Lajtha, *Science* **1973**, *181*, 949.

[3] a) F. Gross, J. Lazar, H. Orth, *Science* **1972**, *175*, 656; b) I. Katoh, T. Yasunaga, Y. Ikawa, Y. Yoshinaka, *Nature* **1987**, *329*, 654; c) J. M. Sayer, J. M. Louis, *Proteins Struct. Funct. Bioinf.* **2009**, *75*, 556.

[4] a) Y. Masuoka, A. Nagai, K. Shin-ya, K. Furihata, K. Nagai, K. Suzuki, Y. Hayakawa, H. Seto, *Tetrahedron Lett.* **2001**, *42*, 41; b) S. J. Crabb, M. Howell, H. Rogers, M. Ishfaq, A. Yurek-George, K. Carey, B. M. Pickering, P. East, R. Mitter, S. Maeda, P. W. Johnson, P. Townsend, K. Shin-ya, M. Yoshida, A. Ganesan, G. Packham, *Biochem. Pharmacol.* **2008**, *76*, 463.

[5] K. L. Rinehart, Jr., J. B. Gloer, R. G. Hughes, Jr., H. E. Renis, J. P. McGovren, E. B. Swynenberg, D. A. Stringfellow, S. L. Kuentzel, L. H. Li, *Science* **1981**, *212*, 933.

[6] a) J. Mccafferty, A. D. Griffiths, G. Winter, D. J. Chiswell, *Nature* **1990**, *348*, 552; b) L. C. Mattheakis, R. R. Bhatt, W. J. Dower, *Proc. Natl. Acad. Sci. USA* **1994**, *91*, 9022; c) N. Nemoto, E. Miyamoto-Sato, Y. Husimi, H. Yanagawa, *FEBS Lett.* **1997**, *414*, 405; d) R. W. Roberts, J. W. Szostak, *Proc. Natl. Acad. Sci. USA* **1997**, *94*, 12297.

[7] a) L. Wang, J. Xie, P. G. Schultz, *Annu. Rev. Biophys. Biomol. Struct.* **2006**, *35*, 225; b) Z. Tan, A. C. Forster, S. C. Blacklow, V. W. Cornish, *J. Am. Chem. Soc.* **2004**, *126*, 12752; c) L. M. Dedkova, N. E. Fahmi, S. Y. Golovine, S. M. Hecht, *J. Am. Chem. Soc.* **2003**, *125*, 6616; d) T. Watanabe, N. Muranaka, I. Iijima, T. Hohsaka, *Biochem. Biophys. Res. Commun.* **2007**, *361*, 794.

[8] a) S. Trobro, J. Aqvist, *Proc. Natl. Acad. Sci. USA* **2005**, *102*, 12395; b) A. Gindulyte, A. Bashan, I. Agmon, L. Massa, A. Yonath, J. Karle, *Proc. Natl. Acad. Sci. USA* **2006**, *103*, 13327; c) R. M. Voorhees, A. Weixlbaumer, D. Loakes, A. C. Kelley, V. Ramakrishnan, *Nat. Struct. Mol. Biol.* **2009**, *16*, 528.

[9] H. Murakami, A. Ohta, H. Ashigai, H. Suga, *Nat. Methods* **2006**, *3*, 357.
[10] Y. Goto, T. Katoh, H. Suga, *Nat. Protoc.* **2011**; in press.
[11] a) Y. Goto, A. Ohta, Y. Sako, Y. Yamagishi, H. Murakami, H. Suga, *ACS Chem. Biol.* **2008**, *3*, 120; b) Y. Goto, H. Murakami, H. Suga, *RNA* **2008**, *14*, 1390; c) Y. Goto, H. Suga, *J. Am. Chem. Soc.* **2009**, *131*, 5040.
[12] a) T. Kawakami, S. Aimoto, *Chem. Lett.* **2007**, *36*, 76; b) T. Kawakami, S. Aimoto, *Tetrahedron Lett.* **2007**, *48*, 1903.
[13] T. Kawakami, A. Ohta, M. Ohuchi, H. Ashigai, H. Murakami, H. Suga, *Nat. Chem. Biol.* **2009**, *5*, 888.
[14] a) S. Luckett, R. S. Garcia, J. J. Barker, A. V. Konarev, P. R. Shewry, A. R. Clarke, R. L. Brady, *J. Mol. Biol.* **1999**, *290*, 525; b) M. L. Korsinczky, H. J. Schirra, D. J. Craik, *Curr. Protein Pept. Sci.* **2004**, *5*, 351.

Received: February 10, 2011
Published online on April 19, 2011

Journal of General Virology (2011), **92**, 2082–2087 DOI 10.1099/vir.0.032391-0

Short Communication

Structural requirements of virion-associated cholesterol for infectivity, buoyant density and apolipoprotein association of hepatitis C virus

Mami Yamamoto,[1,2] Hideki Aizaki,[1] Masayoshi Fukasawa,[3] Tohru Teraoka,[2] Tatsuo Miyamura,[1] Takaji Wakita[1] and Tetsuro Suzuki[1,4]

Correspondence
Tetsuro Suzuki
tesuzuki@hama-med.ac.jp

[1]Department of Virology II, National Institute of Infectious Diseases, Toyama 1-23-1, Shinjuku-ku, Tokyo 162-8640, Japan

[2]United Graduate School of Agricultural Science, Tokyo University of Agriculture and Technology, Saiwai-cho 3-5-8, Fuchu, Tokyo 183-8509, Japan

[3]Department of Biochemistry and Cell Biology, National Institute of Infectious Diseases, Toyama 1-23-1, Shinjuku-ku, Tokyo 162-8640, Japan

[4]Department of Infectious Diseases, Hamamatsu University School of Medicine, Handayama 1-20-1, Higashi-ku, Hamamatsu 431-3192, Japan

Received 22 March 2011
Accepted 17 May 2011

Our earlier study has demonstrated that hepatitis C virus (HCV)-associated cholesterol plays a key role in virus infectivity. In this study, the structural requirement of sterols for infectivity, buoyant density and apolipoprotein association of HCV was investigated further. We removed cholesterol from virions with methyl β-cyclodextrin, followed by replenishment with 10 exogenous cholesterol analogues. Among the sterols tested, dihydrocholesterol and coprostanol maintained the buoyant density of HCV and its infectivity, and 7-dehydrocholesterol restored the physical appearance of HCV, but suppressed its infectivity. Other sterol variants with a 3β-hydroxyl group or with an aliphatic side chain did not restore density or infectivity. We also provide evidence that virion-associated cholesterol contributes to the interaction between HCV particles and apolipoprotein E. The molecular basis for the effects of different sterols on HCV infectivity is discussed.

Hepatitis C virus (HCV) is a major cause of liver diseases, and is an enveloped, plus-strand RNA virus of the genus *Hepacivirus* of the family *Flaviviridae*. The mature HCV virion is considered to consist of a nucleocapsid, an outer envelope composed of the viral E1 and E2 proteins and a lipid membrane. Production and infection of several enveloped viruses, such as human immunodeficiency virus type 1 (HIV-1), hepatitis B virus and varicella-zoster virus (Bremer *et al.*, 2009; Campbell *et al.*, 2001; Graham *et al.*, 2003; Hambleton *et al.*, 2007), are dependent on cholesterol associated with virions. However, except for HIV-1 (Campbell *et al.*, 2002, 2004), there is limited information about the effects of replacing cholesterol with sterol analogues on the virus life cycle. We demonstrated the higher cholesterol content of HCV particles compared with host-cell membranes, and that HCV-associated cholesterol plays a key role in virion maturation and infectivity (Aizaki *et al.*, 2008). Recently, by using mass spectrometry, Merz *et al.* (2011) identified cholesteryl esters, cholesterol, phosphatidylcholine and sphingomyelin as major lipids of purified HCV particles.

To investigate further the effect of the structural requirement for cholesterol on the infectivity, buoyant density and apolipoprotein association of HCV, depletion of virion-associated cholesterol and substitution of endogenous cholesterol with structural analogues (Fig. 1a) was used in this study. HCVcc (HCV grown in cell culture) of the JFH-1 isolate (Wakita *et al.*, 2005), prepared as described previously (Aizaki *et al.*, 2008), was treated with 1 mM methyl β-cyclodextrin (B-CD), which extracts cholesterol from biological membranes, for 1 h at 37 °C. The cholesterol-depleted virus was then incubated with exogenous cholesterol or cholesterol analogues at various concentrations for 1 h. After removal of B-CD and free sterols by centrifugation at 38 000 r.p.m. (178 000 ***g***) for 2.5 h, the treated particles were used to infect Huh7 cells, kindly provided by Dr Francis V. Chisari (The Scripps Research Institute, La Jolla, CA, USA), and their infectivity was determined by quantifying the viral core protein in cells using an enzyme immunoassay (Ortho-Clinical Diagnostics) at 3 days post-infection (p.i.). Virus infectivity, which fell to <20 % after B-CD treatment, was

A supplementary table and figure are available with the online version of this paper.

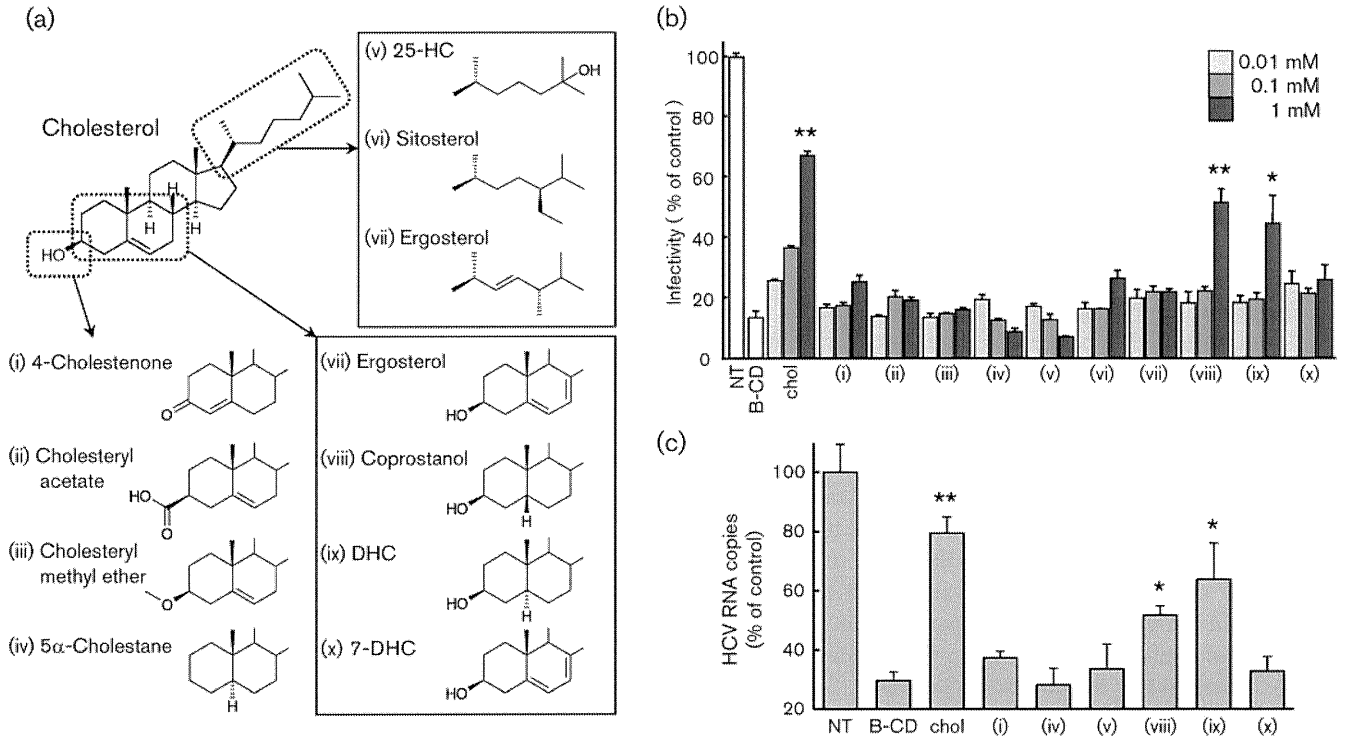

Fig. 1. Role of virion-associated cholesterol analogues in virus infection. (a) Structures of sterols used in this study. Variations in the 3β-hydroxyl group (lower left), aliphatic side chain (upper right) or ring structure (lower right) of cholesterol are shown. (i–x) Compounds studied in (b) and (c). (b) Effect of replenishment with sterols on HCV infectivity. Intracellular HCV core levels were determined at 72 h p.i. as the indicator of infectivity, which is represented as a percentage of the untreated HCVcc level (NT). (c) Effects of virion-associated sterols on virus internalization. HCV RNA copies in cells after virus internalization were quantified and are shown as percentages of the untreated HCVcc level (NT). (b, c) Means+SD of four samples are shown. *P<0.05; **P<0.01, compared with B-CD-treated virus (unpaired Student's t-test). Data are representative of at least two experiments.

recovered by addition of cholesterol at 0.01–1 mM in a dose-dependent manner (Fig. 1b). Among the cholesterol analogues tested, variants with a 3β-hydroxyl group (4-cholestenone, cholesteryl acetate, cholesteryl methyl ether and 5α-cholestane) or variants with an aliphatic side chain [25-hydroxycholesterol (25-HC), sitosterol and ergosterol] exhibited no or little effect on the recovery of infectivity of B-CD-treated HCV (Fig. 1b, lanes i–vii). In contrast, addition of variants in the structure of the sterol rings [coprostanol or dihydrocholesterol (DHC)] at 1 mM restored infectivity to around 50 % compared with non-treated virus control (Fig. 1b, lanes viii and ix). Other variants in the ring structure [7-dehydrocholesterol (7-DHC) and ergosterol, which is also a variant with an aliphatic side chain as indicated above] did not show any increase in the infectivity of B-CD-treated virus (Fig. 1b, lanes x and vii).

We demonstrated previously that HCV-associated cholesterol plays an important role in the internalization step of the virus, but not in cell attachment during virus entry (Aizaki *et al.*, 2008). The effect of virion-associated cholesterol analogues on virus attachment to cells and following internalization was determined. HCVcc, treated with B-CD with or without subsequent replenishment with sterols, was incubated with Huh7-25-CD81 cells, which stably express CD81 (Akazawa *et al.*, 2007), for 1 h at 4 °C. As an internalization assay, the incubation temperature was shifted to 37 °C post-binding procedure and maintained for 2 h. The cells were then treated with 0.25 % trypsin for 10 min at 37 °C, by which >90 % of HCV bound to the cell surface was removed (data not shown; Aizaki *et al.*, 2008). Internalized HCV was quantified by measuring the viral RNA in cell lysates by real-time RT-PCR (Takeuchi *et al.*, 1999). B-CD treatment or supplementation with sterols of B-CD-treated HCV had little or no effect on virus attachment to the cell surface (data not shown). Regarding virus internalization (Fig. 1c), treatment of HCVcc with 1 mM B-CD resulted in approximately 70 % reduction of viral RNA. The reduced level of the internalized HCV recovered markedly to approximately 80 % of the untreated HCVcc level by replenishment with 1 mM cholesterol. In agreement with the results shown in Fig. 1(b), addition of coprostanol or DHC to the B-CD-treated virus caused a significant recovery of virus internalization, suggesting that coprostanol and DHC associated with the

virion have the ability to play a role in HCV internalization into cells, in a manner comparable to cholesterol (Fig. 1c, lanes viii and ix). No or only a little recovery of virus internalization was observed by loading with other cholesterol analogues, such as 4-cholestenone, 5α-cholestane, 25-HC or 7-DHC (Fig. 1c, lanes i, iv, v and x).

To monitor the effect of cholesterol analogues on the physical characteristics of HCV, we next investigated buoyant-density profiles by using sucrose density-gradient centrifugation, in which untreated, B-CD-treated and sterol-replenished HCVcc were concentrated and layered onto continuous 10–60 % (w/v) sucrose density gradients, followed by centrifugation at 35 000 r.p.m. (151 000 ***g***) for 14 h. Fractions were collected and analysed for the core protein. Fig. 2 shows that the virus density became higher after treatment with B-CD and that cholesterol-replenished virus shifted the density of B-CD-treated HCV to the non-treated level. Consistent with the result shown in Fig. 1(b), no effect on restoration of the buoyant densities of HCV was observed using variants with modifications in either the 3β-hydroxyl group (4-cholestenone, cholesteryl acetate and 5α-cholestane) or the aliphatic side chain (25-HC and sitosterol). In contrast, variants in the sterol ring structure (coprostanol, DHC and 7-DHC) had an ability to recover the density of B-CD-treated virus to that of non-treated virus.

Incorporation efficiency of the sterols into the cholesterol-depleted HCVcc was further determined by gas chromatography with flame ionization detection (see Supplementary Table S1, available in JGV Online). Under the experimental conditions used, exogenously supplied cholesterol after B-CD treatment was able to restore cholesterol content in HCVcc almost to initial levels. When 4-cholestenone, cholesteryl acetate, 25-HC, DHC or 7-DHC was added to B-CD-treated HCVcc, virion-associated sterol levels were 146, 157, 68, 96 or 73 %, respectively, of that of the non-treated control. The proportion of cholesterol analogues to the total sterols incorporated was ⩾30 % when 4-cholestenone, cholesteryl acetate, DHC or 7-DHC was used; however, the proportion in the case of 25-HC was only 3 %. It may be that the hydrophilic modification of the aliphatic side chain leads to poor association with HCVcc.

Collectively, exogenous variants with the 3β-hydroxyl group, such as 4-cholestenone and cholesteryl acetate, can be incorporated into B-CD-treated HCVcc, but resulted in no recovery of virus infectivity, indicating the importance of the 3β-hydroxyl group of cholesterol associated with the virus envelope in HCV infectivity. In contrast, two variants with modification in their sterol ring structures, coprostanol and DHC, have the ability to substitute for cholesterol. However, 7-DHC, another variant within the sterol ring, is incorporated readily into the depleted virion and restores the virus density, HCV replenished with 7-DHC is not infectious. These facts suggest that reduced forms of the sterol ring (coprostanol and DHC) in virion-associated cholesterol can be permitted for maintaining virus infectivity. However, a molecule with an additional double bond in the ring structure (7-DHC) seems to fail to exhibit infectivity, presumably because the change reduces structural flexibility in the

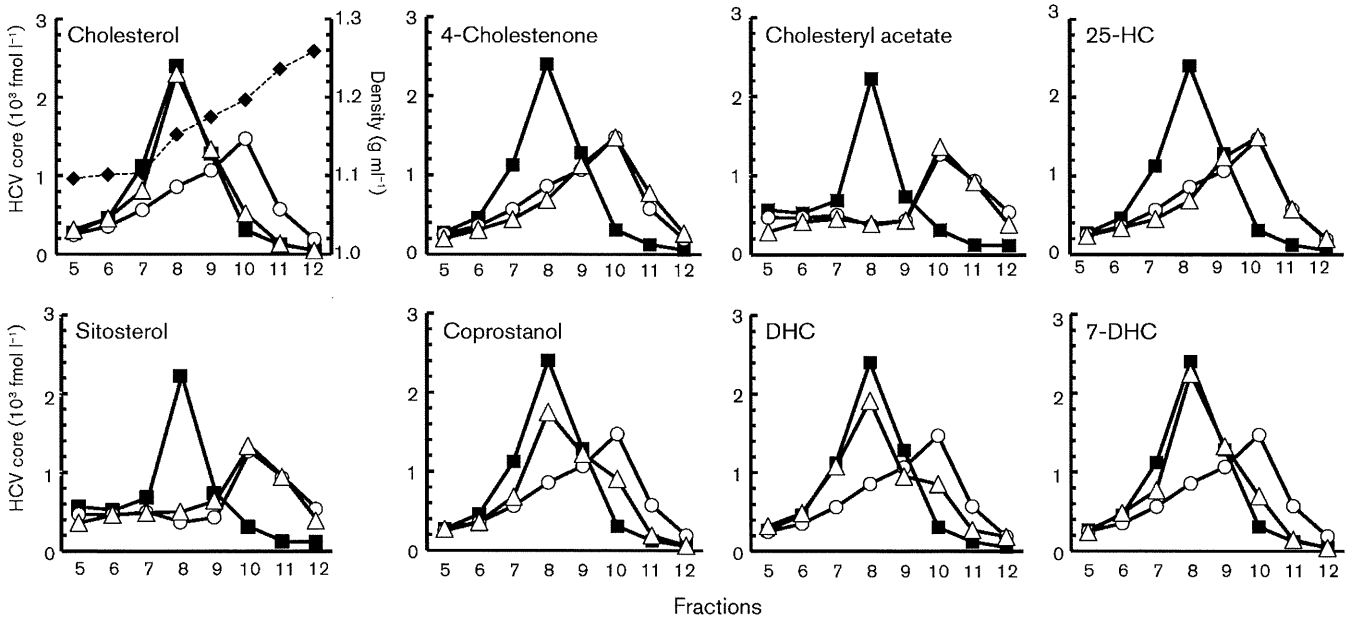

Fig. 2. Sucrose density-gradient profiles of lipid-modified HCV. Core protein concentration in each fraction of untreated HCVcc (■), B-CD-treated HCVcc (○) or HCVcc replenished with sterols (△) was determined. Corresponding densities of fractions are shown as a dashed line (◆).

sterol molecule and consequently in the virion structure. Coprostanol and DHC are *cis* and *trans* isomers, which are often known to have different physical properties. However, based on their molecular models, these two sterols, as well as cholesterol, possibly have similar spatial arrangements of the aliphatic side chain, the hydroxyl group and four-ring region because of their structural flexibility. In contrast, the spatial arrangement of 7-DHC does not seem comparable to that of cholesterol. Campbell *et al.* (2004) reported that replacement of HIV-1-associated cholesterol with raft-inhibiting sterols, including coprostanol, suppresses HIV-1 infectivity, whereas replacement with raft-promoting analogues such as DHC and 7-DHC (Megha *et al.*, 2006; Wang *et al.*, 2004; Xu & London, 2000; Xu *et al.*, 2001) maintains infectivity, demonstrating the importance of the raft-promoting properties of virion-associated cholesterol in HIV-1 infectivity (Campbell *et al.*, 2004). It is therefore likely that HCV-associated cholesterol is involved, at least in part, in virus infectivity via a molecular basis independent of lipid-raft formation.

The density of blood-circulating HCV is heterogeneous, ranging approximately from <1.06 to 1.25 g ml^{-1}, and it is proposed that low-density virus is associated with very-low-density lipoprotein (VLDL) and/or low-density lipoprotein (LDL) (André *et al.*, 2002; Thomssen *et al.*, 1993). It has recently been demonstrated that the pathway for VLDL assembly plays a role in assembly and maturation of infectious HCVcc (Icard *et al.*, 2009). HCVcc with low density, which is presumably associated with VLDL or VLDL-like lipoproteins, was found to possess higher infectivity than that with high density (Lindenbach *et al.*, 2006). This study, as well as our earlier work, indicated that removal of cholesterol from HCVcc by B-CD increased the buoyant density of the virus and reduced its infectivity. Thus, one may hypothesize that the virion-associated cholesterol plays a role in the formation of a complex with lipoproteins or apolipoproteins. To address this, the interaction between apolipoproteins and HCVcc with or without B-CD treatment was investigated by co-immunoprecipitation (Co-IP kit; Thermo Scientific). Virus samples were subjected separately to AminoLink Plus coupling resin, which was conjugated with a monoclonal antibody (mAb) against apolipoprotein E (ApoE) or apolipoprotein B (ApoB), and incubated at 4 °C for 4 h. After washing, total RNAs were extracted from the resulting resin beads by using TRIzol reagent (Invitrogen), followed by quantification of HCV RNA as described above (Takeuchi *et al.*, 1999). As indicated in Fig. 3(a), only a fraction of HCVcc was precipitated with an anti-ApoB mAb. In contrast, an anti-ApoE mAb was able to coprecipitate a considerable amount of the virus. It is of interest that B-CD-treated HCVcc hardly reacted with the mAb; however, the cholesterol-replenished virus was found to recover its reactivity, suggesting a role for virion-associated cholesterol in the formation of the HCV–lipoprotein/apolipoprotein complex. The results obtained are consistent with findings indicating that HCVcc can be captured with anti-ApoE antibodies, but capture with anti-ApoB antibodies is inefficient (Chang *et al.*, 2007; Hishiki *et al.*, 2010; Huang *et al.*, 2007; Jiang & Luo, 2009; Merz *et al.*, 2011; Nielsen *et al.*, 2006; Owen *et al.*, 2009), as well as with a recent model of structures of infectious HCV, in which HCVcc looks like ApoE-positive and primarily ApoB-negative lipoproteins (Bartenschlager *et al.*, 2011). We further tested the ApoE distribution in the density-gradient fractions of HCVcc samples (see Supplementary Fig. S1, available in JGV Online). With or without cholesterol depletion, ApoE was detected at a wide range of concentrations: 1.04 g ml^{-1} (fraction 1) to 1.17 g ml^{-1} (fraction 9). However, its level in the fractions at 1.10 g ml^{-1} (fraction 5) to approximately 1.17 g ml^{-1} was moderately decreased in the case of B-CD-treated virus.

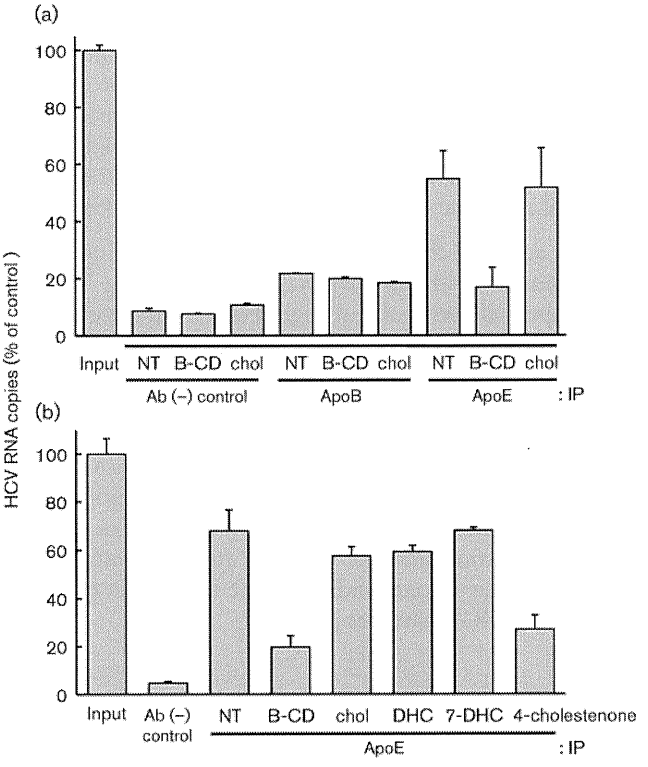

Fig. 3. Effect of virion-associated sterols on HCV–apolipoprotein interaction. (a) HCVcc samples with no treatment (NT), B-CD-treated (B-CD) or replenished with cholesterol (chol) were incubated with an amine-reactive resin coupling either an anti-ApoB mAb (ApoB) or an anti-ApoE mAb (ApoE). Control resin that is composed of the same material as above, but is not activated, was used as a negative control [Ab (–) control]. (b) B-CD-treated HCVcc was incubated with cholesterol (chol), DHC, 7-DHC or 4-cholestenone, followed by immunoprecipitation with the resin coupling with anti-ApoE mAb. (a, b) HCV RNAs in the immunoprecipitates were quantified and are indicated as percentages of the amount of input HCVcc RNA. Means+SD of three samples are shown. Data are representative of three experiments.

Whether cholesterol analogues could have a comparable role in HCV association with lipoprotein was examined further (Fig. 3b). Addition of DHC or 7-DHC, but not 4-cholestenone, to B-CD-treated HCVcc resulted in the recovery of coprecipitation of the virus with anti-ApoE. The results are correlated with the effect of sterols on the restoration of the buoyant densities of lipid-modified HCVcc (Fig. 2), suggesting that virion-associated cholesterol variants with modification in the sterol rings, but not in either the 3β-hydroxyl group or the aliphatic side chain, may tolerate the interaction between HCV and ApoE-positive lipoprotein.

Given that 7-DHC restored the association of HCV with ApoE and virion buoyant density, but did not restore infectivity, cholesterol and/or its analogues might affect the ability of virion membranes to fuse with the cell, independent of ApoE association. As cholesterol is an important mediator of membrane fluidity, one may hypothesize that HCV-associated cholesterol is involved in infectivity through modulation of the membrane fluidity. It has been reported that, in patients with Smith–Lemli–Opitz syndrome, a disorder of the cholesterol-synthesis pathway, cholesterol content decreases and 7-DHC increases in the cell membranes, leading to alteration of phospholipid packing in the membrane and abnormal membrane fluidity (Tulenko *et al.*, 2006).

It is now accepted that maturation and release of infectious HCV coincide with the pathway for producing VLDLs, which export cholesterol and triglyceride from hepatocytes. This study revealed roles for the structural basis of virion-associated cholesterol in the infectivity, buoyant density and apolipoprotein association of HCV. Although it was shown that HCV virions in infected patients, so-called lipo–viro particles, exhibited certain biochemical properties such as containing ApoB, ApoC and ApoE (Diaz *et al.*, 2006; Bartenschlager *et al.*, 2011), our studies provide useful information and the basis for future investigations toward a deeper understanding of the biogenesis pathway of infectious HCV particles.

Acknowledgements

We thank M. Matsuda, M. Sasaki and T. Date for technical assistance and T. Mizoguchi for secretarial work. This work was partially supported by a grant-in-aid for Scientific Research from the Japan Society for the Promotion of Science, from the Ministry of Health, Labor, and Welfare of Japan, and from the Ministry of Education, Culture, Sports, Science, and Technology.

References

Aizaki, H., Morikawa, K., Fukasawa, M., Hara, H., Inoue, Y., Tani, H., Saito, K., Nishijima, M., Hanada, K. & other authors (2008). Critical role of virion-associated cholesterol and sphingolipid in hepatitis C virus infection. *J Virol* **82**, 5715–5724.

Akazawa, D., Date, T., Morikawa, K., Murayama, A., Miyamoto, M., Kaga, M., Barth, H., Baumert, T. F., Dubuisson, J. & Wakita, T. (2007). CD81 expression is important for the permissiveness of Huh7 cell clones for heterogeneous hepatitis C virus infection. *J Virol* **81**, 5036–5045.

André, P., Komurian-Pradel, F., Deforges, S., Perret, M., Berland, J. L., Sodoyer, M., Pol, S., Bréchot, C., Paranhos-Baccalà, G. & Lotteau, V. (2002). Characterization of low- and very-low-density hepatitis C virus RNA-containing particles. *J Virol* **76**, 6919–6928.

Bartenschlager, R., Penin, F., Lohmann, V. & André, P. (2011). Assembly of infectious hepatitis C virus particles. *Trends Microbiol* **19**, 95–103.

Bremer, C. M., Bung, C., Kott, N., Hardt, M. & Glebe, D. (2009). Hepatitis B virus infection is dependent on cholesterol in the viral envelope. *Cell Microbiol* **11**, 249–260.

Campbell, S. M., Crowe, S. M. & Mak, J. (2001). Lipid rafts and HIV-1: from viral entry to assembly of progeny virions. *J Clin Virol* **22**, 217–227.

Campbell, S. M., Crowe, S. M. & Mak, J. (2002). Virion-associated cholesterol is critical for the maintenance of HIV-1 structure and infectivity. *AIDS* **16**, 2253–2261.

Campbell, S., Gaus, K., Bittman, R., Jessup, W., Crowe, S. & Mak, J. (2004). The raft-promoting property of virion-associated cholesterol, but not the presence of virion-associated Brij 98 rafts, is a determinant of human immunodeficiency virus type 1 infectivity. *J Virol* **78**, 10556–10565.

Chang, K. S., Jiang, J., Cai, Z. & Luo, G. (2007). Human apolipoprotein E is required for infectivity and production of hepatitis C virus in cell culture. *J Virol* **81**, 13783–13793.

Diaz, O., Delers, F., Maynard, M., Demignot, S., Zoulim, F., Chambaz, J., Trépo, C., Lotteau, V. & André, P. (2006). Preferential association of hepatitis C virus with apolipoprotein B48-containing lipoproteins. *J Gen Virol* **87**, 2983–2991.

Graham, D. R., Chertova, E., Hilburn, J. M., Arthur, L. O. & Hildreth, J. E. (2003). Cholesterol depletion of human immunodeficiency virus type 1 and simian immunodeficiency virus with β-cyclodextrin inactivates and permeabilizes the virions: evidence for virion-associated lipid rafts. *J Virol* **77**, 8237–8248.

Hambleton, S., Steinberg, S. P., Gershon, M. D. & Gershon, A. A. (2007). Cholesterol dependence of varicella-zoster virion entry into target cells. *J Virol* **81**, 7548–7558.

Hishiki, T., Shimizu, Y., Tobita, R., Sugiyama, K., Ogawa, K., Funami, K., Ohsaki, Y., Fujimoto, T., Takaku, H. & other authors (2010). Infectivity of hepatitis C virus is influenced by association with apolipoprotein E isoforms. *J Virol* **84**, 12048–12057.

Huang, H., Sun, F., Owen, D. M., Li, W., Chen, Y., Gale, M., Jr & Ye, J. (2007). Hepatitis C virus production by human hepatocytes dependent on assembly and secretion of very low-density lipoproteins. *Proc Natl Acad Sci U S A* **104**, 5848–5853.

Icard, V., Diaz, O., Scholtes, C., Perrin-Cocon, L., Ramière, C., Bartenschlager, R., Penin, F., Lotteau, V. & André, P. (2009). Secretion of hepatitis C virus envelope glycoproteins depends on assembly of apolipoprotein B positive lipoproteins. *PLoS One* **4**, e4233.

Jiang, J. & Luo, G. (2009). Apolipoprotein E but not B is required for the formation of infectious hepatitis C virus particles. *J Virol* **83**, 12680–12691.

Lindenbach, B. D., Meuleman, P., Ploss, A., Vanwolleghem, T., Syder, A. J., McKeating, J. A., Lanford, R. E., Feinstone, S. M., Major, M. E. & other authors (2006). Cell culture-grown hepatitis C virus is infectious *in vivo* and can be recultured *in vitro*. *Proc Natl Acad Sci U S A* **103**, 3805–3809.

Megha, Bakht, O. & London, E. (2006). Cholesterol precursors stabilize ordinary and ceramide-rich ordered lipid domains (lipid

rafts) to different degrees. Implications for the Bloch hypothesis and sterol biosynthesis disorders. *J Biol Chem* **281**, 21903–21913.

Merz, A., Long, G., Hiet, M. S., Brügger, B., Chlanda, P., Andre, P., Wieland, F., Krijnse-Locker, J. & Bartenschlager, R. (2011). Biochemical and morphological properties of hepatitis C virus particles and determination of their lipidome. *J Biol Chem* **286**, 3018–3032.

Nielsen, S. U., Bassendine, M. F., Burt, A. D., Martin, C., Pumeechockchai, W. & Toms, G. L. (2006). Association between hepatitis C virus and very-low-density lipoprotein (VLDL)/LDL analyzed in iodixanol density gradients. *J Virol* **80**, 2418–2428.

Owen, D. M., Huang, H., Ye, J. & Gale, M., Jr (2009). Apolipoprotein E on hepatitis C virion facilitates infection through interaction with low-density lipoprotein receptor. *Virology* **394**, 99–108.

Takeuchi, T., Katsume, A., Tanaka, T., Abe, A., Inoue, K., Tsukiyama-Kohara, K., Kawaguchi, R., Tanaka, S. & Kohara, M. (1999). Real-time detection system for quantification of hepatitis C virus genome. *Gastroenterology* **116**, 636–642.

Thomssen, R., Bonk, S. & Thiele, A. (1993). Density heterogeneities of hepatitis C virus in human sera due to the binding of beta-lipoproteins and immunoglobulins. *Med Microbiol Immunol (Berl)* **182**, 329–334.

Tulenko, T. N., Boeze-Battaglia, K., Mason, R. P., Tint, G. S., Steiner, R. D., Connor, W. E. & Labelle, E. F. (2006). A membrane defect in the pathogenesis of the Smith–Lemli–Opitz syndrome. *J Lipid Res* **47**, 134–143.

Wakita, T., Pietschmann, T., Kato, T., Date, T., Miyamoto, M., Zhao, Z., Murthy, K., Habermann, A., Kräusslich, H. G. & other authors (2005). Production of infectious hepatitis C virus in tissue culture from a cloned viral genome. *Nat Med* **11**, 791–796.

Wang, J., Megha & London, E. (2004). Relationship between sterol/steroid structure and participation in ordered lipid domains (lipid rafts): implications for lipid raft structure and function. *Biochemistry* **43**, 1010–1018.

Xu, X. & London, E. (2000). The effect of sterol structure on membrane lipid domains reveals how cholesterol can induce lipid domain formation. *Biochemistry* **39**, 843–849.

Xu, X., Bittman, R., Duportail, G., Heissler, D., Vilcheze, C. & London, E. (2001). Effect of the structure of natural sterols and sphingolipids on the formation of ordered sphingolipid/sterol domains (rafts). Comparison of cholesterol to plant, fungal, and disease-associated sterols and comparison of sphingomyelin, cerebrosides, and ceramide. *J Biol Chem* **276**, 33540–33546.

Hepatitis C Virus Reveals a Novel Early Control in Acute Immune Response

Noëlla Arnaud[1], Stéphanie Dabo[1], Daisuke Akazawa[2], Masayoshi Fukasawa[3], Fumiko Shinkai-Ouchi[3], Jacques Hugon[4], Takaji Wakita[2], Eliane F. Meurs[1]*

1 Institut Pasteur, Hepacivirus and Innate Immunity, Paris, France, **2** National Institute of Infectious Diseases, Department of Virology II, Tokyo, Japan, **3** National Institute of Infectious Diseases, Department of Biochemistry and Cell Biology, Tokyo, Japan, **4** Institut du Fer à Moulin, INSERM UMRS 839, Paris, France

Abstract

Recognition of viral RNA structures by the intracytosolic RNA helicase RIG-I triggers induction of innate immunity. Efficient induction requires RIG-I ubiquitination by the E3 ligase TRIM25, its interaction with the mitochondria-bound MAVS protein, recruitment of TRAF3, IRF3- and NF-κB-kinases and transcription of Interferon (IFN). In addition, IRF3 alone induces some of the Interferon-Stimulated Genes (ISGs), referred to as early ISGs. Infection of hepatocytes with Hepatitis C virus (HCV) results in poor production of IFN despite recognition of the viral RNA by RIG-I but can lead to induction of early ISGs. HCV was shown to inhibit IFN production by cleaving MAVS through its NS3/4A protease and by controlling cellular translation through activation of PKR, an eIF2α-kinase containing dsRNA-binding domains (DRBD). Here, we have identified a third mode of control of IFN induction by HCV. Using HCVcc and the Huh7.25.CD81 cells, we found that HCV controls RIG-I ubiquitination through the di-ubiquitine-like protein ISG15, one of the early ISGs. A transcriptome analysis performed on Huh7.25.CD81 cells silenced or not for PKR and infected with JFH1 revealed that HCV infection leads to induction of 49 PKR-dependent genes, including ISG15 and several early ISGs. Silencing experiments revealed that this novel PKR-dependent pathway involves MAVS, TRAF3 and IRF3 but not RIG-I, and that it does not induce IFN. Use of PKR inhibitors showed that this pathway requires the DRBD but not the kinase activity of PKR. We then demonstrated that PKR interacts with HCV RNA and MAVS prior to RIG-I. In conclusion, HCV recruits PKR early in infection as a sensor to trigger induction of several IRF3-dependent genes. Among those, ISG15 acts to negatively control the RIG-I/MAVS pathway, at the level of RIG-I ubiquitination.These data give novel insights in the machinery involved in the early events of innate immune response.

Citation: Arnaud N, Dabo S, Akazawa D, Fukasawa M, Shinkai-Ouchi F, et al. (2011) Hepatitis C Virus Reveals a Novel Early Control in Acute Immune Response. PLoS Pathog 7(10): e1002289. doi:10.1371/journal.ppat.1002289

Editor: Aleem Siddiqui, University of California, San Diego, United States of America

Received April 5, 2011; **Accepted** August 13, 2011; **Published** October 13, 2011

Funding: NA was supported by a graduate fellowship from the Ministry of Research and Technology. The work was supported by grants from the Pasteur Institute and by grant R750159 from ANRS (Agence Nationale de la Recherche sur le SIDA et les Hepatites Virales):http://www.anrs.fr The funders had no role in study design, data collection and analysis, decision to publish, or preparation of the manuscript.

Competing Interests: The authors have declared that no competing interests exist.

* E-mail: emeurs@pasteur.fr

Introduction

IFN induction in response to several RNA viruses involves the intracytosolic pathogen recognition receptor (PRR) CARD-containing DexD/H RNA helicase RIG-I. Following its binding to viral RNA, RIG-I undergoes a change in its conformation through Lys63-type ubiquitination by the E3 ligase TRIM25. This allows its N-terminal CARD domain to interact with the CARD domain of the mitochondria-bound adapter MAVS [1,2]. MAVS then interacts with TRAF3 to further recruit downstream IRF3 and NF-κB-activating kinases, that stimulate the IFNβ promoter in a cooperative manner. In addition, IRF3 stimulates directly the promoters of some interferon-induced genes (early ISGs) while NF-κB stimulates that of inflammatory cytokines [3].

The RNA of Hepatitis C virus (HCV) has an intrinsic ability to trigger IFNβ induction through RIG-I [4,5,6]. Yet HCV is a poor IFN inducer. One reason for this comes from the ability of its NS3 protease to cleave MAVS [7]. Another relates to the ability of HCV to trigger activation of the dsRNA-dependent eIF2α kinase PKR [8,9] which leads to inhibition of IFN expression through general control of translation while the viral genome can be translated from its eIF2α-insensitive IRES structure [8].

HCV infection can trigger important intrahepatic synthesis of several IFN-induced genes (ISGs) in patients [10,11] and in animal models of infection in chimpanzees [12]. Expression of ISGs can be explained at least in part by the ability of HCV to activate the IFN-producing pDCs in the liver through cell-to-cell contact with HCV-infected cells [13]. Intriguingly, despite the recognized antiviral activity of a number of these ISGs, their high expression paradoxically represents a negative predictive marker for the response of these patients to standard combination IFN/ribavirin therapy [14,15,16]. The ubiquitine-like protein ISG15 is among the ISGs which are the most highly induced by HCV [16] and was recently shown to act as a pro-HCV agent [17]. Interestingly, ISG15 was also shown to control RIG-I activity through ISGylation [18].

Here, we show that HCV controls IFN induction at the level of RIG-I ubiquitination through the ubiquitine-like protein ISG15, one of the early ISGs. Use of small interfering RNA (siRNA) targeting to compare the effect of ISG15 to that of PKR on IFN induction and HCV replication led to the unexpected finding that HCV infection triggers induction of ISG15 and other ISGs by using PKR as an adapter through its N terminal dsRNA binding domain. This recruits a signaling pathway which involves MAVS,TRAF3

Author Summary

Hepatitis C Virus (HCV) is a poor interferon (IFN) inducer, despite recognition of its RNA by the cytosolic RNA helicase RIG-I. This is due in part through cleavage of MAVS, a downstream adapter of RIG-I, by the HCV NS3/4A protease and through activation of the eIF2α-kinase PKR to control IFN translation. Here, we show that HCV also inhibits RIG-I activation through the ubiquitin-like protein ISG15 and that HCV triggers rapid induction of 49 genes, including ISG15, through a novel signaling pathway that precedes RIG-I and involves PKR as an adapter to recruit MAVS. Hence, we propose to divide the acute response to HCV infection into one early (PKR) and one late (RIG-I) phase, with the former controlling the latter. Furthermore, these data emphazise the need to check compounds designed as immune adjuvants for activation of the early acute phase before using them to sustain innate immunity.

and IRF3 but not RIG-I. Altogether, our results present a novel mechanism by which HCV uses PKR and ISG15 to attenuate the innate immune response.

Results

HCV infection negatively controls RIG-I ubiquitination

We recently reported that the HCV permissive Huh7.25.CD81 cells [19] that we used to identify the pro-HCV action of PKR, did not induce IFN in response to HCV infection, unless after ectopic expression of TRIM25 [8]. We started this study by investigating at which level this defect could occur. A $P_{358}L$ substitution in the endogenous TRIM25 of these cells, revealed by sequence analysis, proved to have no incidence of the ability of TRIM25 to participate in the IFN induction process. Indeed, ectopic expression of a TRIM25 $P_{358}L$ construct was as efficient as a TRIM25wt construct to increase IFN induction in the Huh7.25.CD81 cells, after infection with Sendai virus (SeV) (**Figure 1A**). Like some other members of the TRIM family, TRIM25 is localized in both the cytosol and nucleus and is induced upon IFN treatment [20]. No specific difference between the cellular localization of TRIM25 was observed in the Huh7.25.CD81 cells when compared to Huh7 cells or Huh7.5 cells, which rules out a role for a cellular mislocalization in its inability to participate in IFN induction (**Figure 1B**). TRIM25 was also efficiently induced by IFN (**Figure 1B and Figure S1**). We assayed whether increasing TRIM25 upon IFN treatment could mimic the effect of its ectopic expression and restore IFN induction in response to HCV infection. However, this resulted only in a poor stimulation of an IFNβ promoter (3 to 5-fold), in contrast to its effect upon SeV infection (230-fold) (**Figure 1C**). Similarly, HCV infection at higher m.o.i, as an attempt to favour recognition of RIG-I by the viral RNA, only modestly increased IFN induction (**Figure 1D**). TRIM25 plays an essential role in IFN induction through RIG-I ubiquitination [1]. We then analysed whether this step was affected by HCV infection in the Huh7.25.CD81 cells. The results showed that, in contrast to SeV infection used as control, HCV infection could not trigger RIG-I ubiquitination, unless the cells are supplied with ectopic TRIM25 (**Figure 1E**). Thus, HCV infection appears to mediate a control on IFN induction through regulation of RIG-I ubiquitination.

HCV controls RIG-I ubiquitination through ISG15

Inhibition of the function of TRIM25 or RIG-I ubiquitination has been suggested to occur via the small ubiquitin-like protein ISG15 and the process of ISGylation [18,21]. We then analysed whether ISG15 was involved in the control of RIG-I ubiquitination upon HCV infection. For this, we chose a transient transfection approach using siRNAs targeting ISG15 in the Huh7.25.CD81 cells. Indeed, this resulted in a strong ubiquitination of RIG-I at 9 hrs and 12 hrs post-HCV infection, which was equivalent to that observed in cells supplied with ectopic TRIM25 (**Figure 2A**). A similar result was obtained after JFH1 infection in the Huh7 cells, used as another HCV-permissive cell line (**Figure S2**). Thus, ISG15 can control RIG-I ubiquitination in different cells infected by HCV. We next investigated whether ISGylation was involved in this process. Absence of detection of RIG-I ubiquitination after HCV infection of the Huh7.25.CD81 cells precludes direct analysis of the effect of ISG15 on RIG-I. We used an IFNβ-luc reporter assay instead, as it proved to be sensitive enough to detect some IFN induction in response to JFH1 infection in those cells (see Figure 1D). We found that IFN induction increased when cells were transfected with siRNAs targeting ISG15 while it decreased in cells overexpressing IGS15 (**Figure 2B**). Expression of ISG15 in the presence of the E1, E2 and E3 ligases involved in ISGylation (respectively Ube1L, UbcH8 and HERC5) [22] further inhibits IFNβ induction (**Figure 2B**). Similar results were observed upon infection with Sendai virus (**Figure S3**). The ISGylation process is strictly dependent on the presence of the E1 ligase Ube1L [23]. Indeed, enhanced IFN promoter activity has been observed in Ube1L−/− cells in response to NDV [18]. In accord with this, depletion of endogenous Ube1L from the Huh7.25.CD81 cells (**Figure S4**), as such or after ectopic expression of ISG15, UbcH8 and HERC5, resulted in an increase in IFNβ induction after infection with HCV (**Figure 2B**). We then analysed the effect of siISG15 on IFNβ induction after infecting the cells with HCV up to 72 hours, in order to pass through the 24 hr time-point where the signaling pathway leading to the transcription of this gene is expected to stop because of the NS3/4A-mediated cleavage of MAVS [8]. The results show that, whereas IFNβ transcription was indeed strongly inhibited after 24 hr in the control cells, it still occurred significantly in the cells expressing siRNA ISG15 (**Figure 2C**). Previous data have shown a positive role for ISG15 on HCV production [24,25]. In accord with this, silencing of ISG15 resulted in clear inhibition of HCV RNA expression with however no significant consequence on the ability of the virions produced to re-infect fresh cells (**Figure 2D**). Analysis of expression of MAVS and NS3, as well as the expression of the core protein as another example of viral protein, then showed that the depletion of ISG15 both decreased and delayed the expression of the viral proteins as compared to the siRNA control cells and that this was correlated by a delay in the NS3/4A-mediated cleavage of MAVS (**Figure 2E**). These results show that ISG15 controls the process of IFN induction during HCV infection by interfering with RIG-I ubiquitination through an ISGylation process and by boosting efficient accumulation of NS3, among other viral proteins, thus favouring its negative control on IFN induction by cleavage of MAVS.

ISG15 strengthens the pro-HCV activity of PKR

ISG15 ([24,25] and this study) and PKR [8,9] emerge as two ISGs with pro-HCV activities, instead of playing an antiviral role. We then assayed the effect of a combined depletion of PKR and ISG15 on HCV replication and IFN expression in the Huh7.25.CD81 cells. As shown in Figure 2 D and B, siRNAs targeting ISG15 were sufficient both to inhibit HCV replication (**Figure 3A**) and to increase IFNβ expression, either measured by RTqPCR (**Figure 3B**) or by using an IFNβ-luciferase reporter

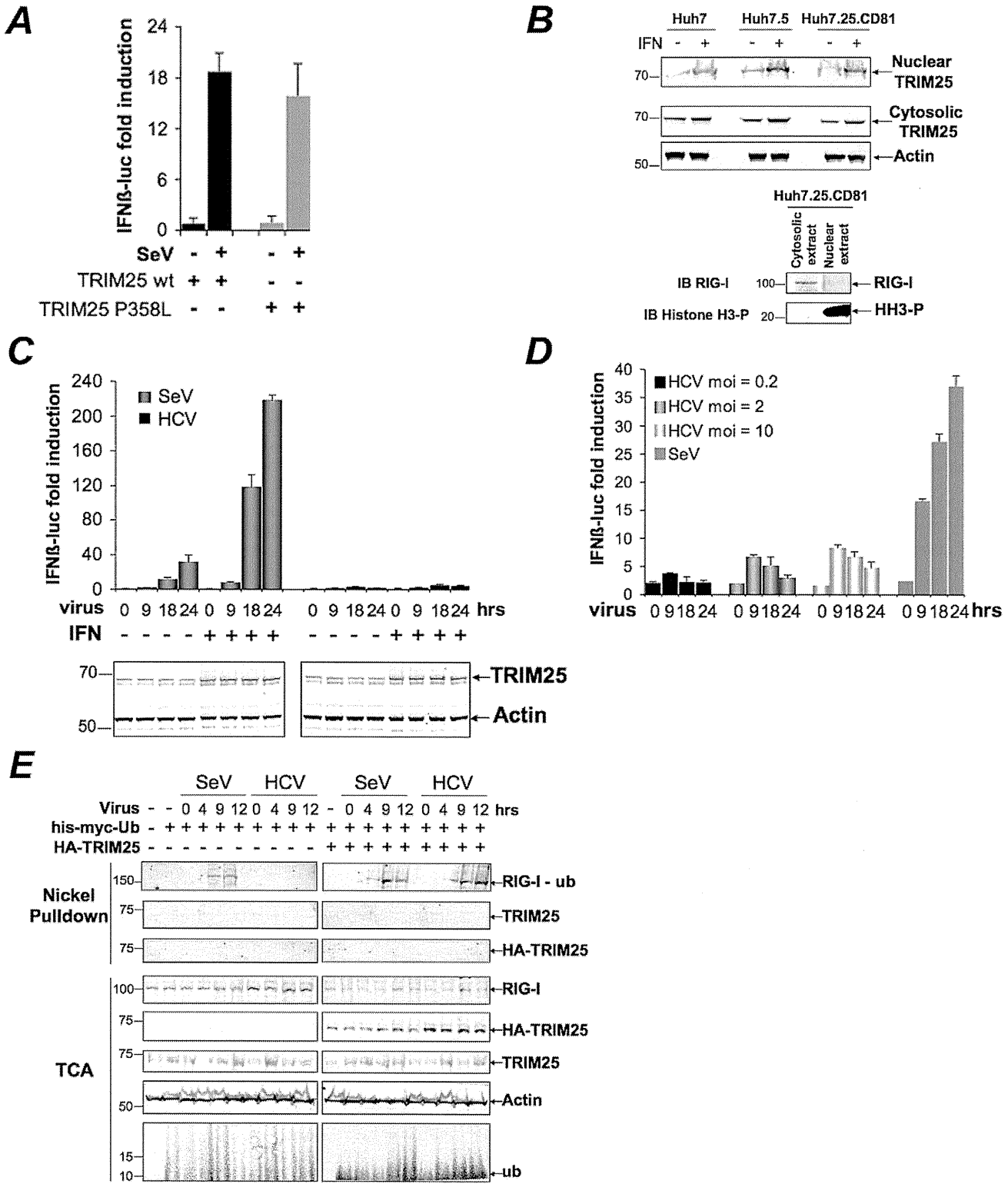

Figure 1. HCV infection negatively controls RIG-I ubiquitination. (**A**) Huh7.25.CD81 cells were transfected for 24 hrs with 150 ng of the pGL2-IFNβ-FLUC; 40 ng of the pRL-TK-RLUC reporter plasmids alone or in presence of 150 ng of a plasmid expressing HA-TRIM25, either as such (TRIM25wt) or containing the $P_{358}L$ substitution (a SNP rs75467764 with no reported pathology). Cells were infected or not with SeV (40 HAU/ml) for 24 hrs. IFN expression was expressed as fold induction of luciferase activity. Error bars represent the mean ± S.D. for triplicates. (**B**) Huh7, Huh7.5 and Huh7.25.CD81 cells were either untreated or treated with 500 U/ml IFNα for 24 hrs. TRIM25 was detected by immunoblot after preparation of nuclear and cytosolic fractions from 25 µg of cell extracts. Detection of Actin, RIG-I and phosphorylated Histone 3 (HH3-P) served as controls. (**C–D**) Huh7.25.CD81 cells were transfected with the reporter plasmids as in A, a few hours before being treated with 500 U/ml IFNα for 24 hrs (**C**) or left untreated (**C or D**). They were then infected with Sendai virus (40 HAU/ml) or with JFH1 at an m.o.i of 0.2 (**C**) or increasing from 0.2 to 10 (**D**). At the times indicated, IFN expression was expressed as fold induction of luciferase activity. Error bars represent the mean ± S.D. for triplicates. Induction of

TRIM25 after IFN treatment was shown by immunoblot (**C**). (**E**) The Huh7.25.CD81 cells were transfected for 48 hrs with 5 μg of His-Myc-Ubiquitin expression plasmid in absence or presence of a plasmid expressing HA-TRIM25 and infected with SeV (40 HAU/ml) or HCV (m.o.i = 6). At the times indicated, 10% of the lysate was precipitated with TCA and the remaining lysate subjected to nickel pulldown under denaturing conditions. Total and ubiquitin (Ub)-modified proteins were separated by SDS-PAGE and revealed by immunoblot.
doi:10.1371/journal.ppat.1002289.g001

assay (**Figure 3C**). Very limited additional effect was observed in the concomitant presence of siRNAs targeting PKR. (**Figure 3B**). Interestingly, we noticed that expression of luciferase from the IFNβ promoter increased throughout the first 18 hours of HCV infection in the siISG15 cells (**Figure 3C**). This was intriguing as it should have been inhibited after 12 hours of HCV infection through the eIF2α kinase activity of PKR and its control on translation [8]. We therefore analysed whether the state of PKR activation (phosphorylation) was dependent on the expression of ISG15. For this, the Huh7.25.CD81 cells were transfected either with siRNAs targeting ISG15 or with a plasmid expressing an HA-ISG15 construct and PKR phosphorylation was analysed as described previously [8]. The results showed that depletion of ISG15 inhibits PKR activation in the HCV-infected cells, while its overexpression stimulates it (**Figure 3D** and **Figure S5**). Therefore these data reveal that, in addition to negatively controlling RIG-I ubiquitination, ISG15 can also positively control PKR activity. The conjugation of both effects results in an efficient control of IFN induction during HCV infection.

HCV triggers a PKR-dependent pathway early in infection to induce ISG15 and other genes

The Huh7.25.CD81 cells express ISG15 at significant basal levels. This situation was not surprising as various cellular systems can also express some of the ISGs at basal level. Expression of ISG15 was approximately 2- and 5-fold higher in the Huh7.25.CD81 cells than in the Huh7.5 or Huh7 cells (data not shown). Intriguingly however, we noticed that ISG15 expression was increased in response to HCV infection (see **Figure 2E**). To investigate this further, we simply re-used the RNAs prepared for the experiment shown in Figure 3B and performed a quantitative kinetics analysis. The results confirmed that HCV can trigger induction of ISG15 (**Figure 4A**). Unexpectedly, analysis of the RNA extracted from the cells treated with siRNAs targeting PKR, revealed that ISG15 RNA expression was strongly repressed when PKR was silenced (**Figure 4A**). This surprising result was confirmed by analysing induction of ISG56, another early ISG [26], both at the level of its endogenous RNA (**Figure 4B**) or by using an ISG56-luciferase vector (**Figure 4C**). In the latter case, a strong increase of the reporter expression in the cells treated with siRNAs targeting ISG15, was similar to the situation observed for IFNβ RNA (**Figure 2B and 2C**). This can be related to activation of the RIG-I pathway, which can function when ISG15 is absent. These data suggest that HCV may use PKR to activate gene transcription. Importantly, this phenomenon was specific to HCV as infection with Sendai virus resulted in a similar induction of ISG15 and ISG56, regardless of PKR (**Figure 4D and Figure S6**). We then examined whether overexpression of PKR could boost induction of ISG15 during HCV infection and how this would affect HCV replication and IFN induction, in relation to the pro-HCV action of ISG15. Huh7.25.CD81 cells were transfected with a plasmid expressing PKR alone or in presence of siRNAs targeting ISG15, before being infected with HCV over 48 hours. Overexpression of PKR increased the ability of HCV to induce ISG15 and concomitantly, led to an increase in HCV RNA expression. The latter increase was abolished when ISG15 was silenced, thus showing that the PKR-dependent increase in HCV expression is mediated by ISG15 (Figure **4E**). However, while the cells silenced for ISG15 are able to induce IFN in response to HCV infection, as shown in Figure 3B, they are unable to do so when PKR is overexpressed. This suggests that PKR may also interfere with the process of IFN induction, independently of ISG15, a possibility that remains to be explored.

A role for PKR in gene induction in response to HCV infection has not been described before. Additional information was therefore obtained through a transcriptome analysis of 2165 genes in the Huh7.25.CD81 cells treated with control siRNAs or siRNAs targeting PKR and infected with HCV for 12 hrs. Out of the most significant 422 genes that were identified, 99 were unmodified or barely modified and 33 were down-regulated, while 290 genes were found to be up-regulated by HCV infection (data not shown). Among those, HCV infection triggered up-regulation of 49 genes which are directly dependent on PKR expression (**Table 1**). Forty percent of these genes (20) belong to the family of the ISGs, with ISG15 among the most induced genes (**Table 1**). In the reciprocal situation, only 17 genes depended on PKR for their down-regulation by HCV infection, with no link to a particular family of genes and limited variation both in number and intensity (**Table S1**). Thus, induction of ISGs upon HCV infection may occur through a novel signaling pathway that involves PKR.

Induction of ISG15 by HCV is independent of RIG-I, involves MAVS/TRAF3 association with PKR and involves the DRBD region but not the catalytic activity of PKR

Infection with RNA viruses or transient transfection with dsRNA can directly and rapidly induce early ISGs, such as ISG15, through IRF3, after activation of the RIG-I/MAVS pathway and recruitment of TRAF3, an essential adapter which recruits the downstream IRF3 kinases TBK1/IKKε. We have shown that the RIG-I pathway was not operative during HCV infection in the Huh7.25.CD81 cells, precisely due to the presence of ISG15. To determine how ISG15 induction through PKR relates to or differs from the RIG-I/MAVS pathway, the Huh7.25.CD81 cells were treated with siRNAs aimed at targeting separately PKR, RIG-I, MAVS, TRAF3 and IRF3 (**Figure S7**) and infected with HCV. The results clearly showed that induction of ISG15 in response to HCV infection depends on PKR, MAVS, TRAF3 and IRF3 but not on RIG-I (**Figure 5A**). The participation of IRF3 was further confirmed by immunofluorescence studies which showed its nuclear translocation at 6 hours post-infection (**Figure S8**). ISG15, as well as ISG56, was also clearly induced in response to HCV infection in two other HCV permissive cell lines, such as Huh7 and Huh7.5 cells, and this induction was abrogated in presence of siRNAs targeting PKR (**Figure 5B and Figure S9**). Importantly, since Huh7.5 cells express a non-functional RIG-I/MAVS pathway due to a mutation in RIG-I, result with these cells supports the notion that the ability of HCV to trigger induction of ISGs through PKR is independent of RIG-I. To have more insights on this novel PKR signaling pathway, PKR was immunoprecipitated at early times points following infection of Huh7.25.CD81 cells with HCV and the immunocomplexes were analysed for the presence of MAVS, TRAF3 and RIG-I. Both MAVS and TRAF3, but not RIG-I, associate with PKR in a time dependent manner, beginning at 2 hrs post-infection (**Figure 5C**). Strikingly, these associations were abrogated by the cell-permeable peptide PRI which is analogous to the first dsRNA binding

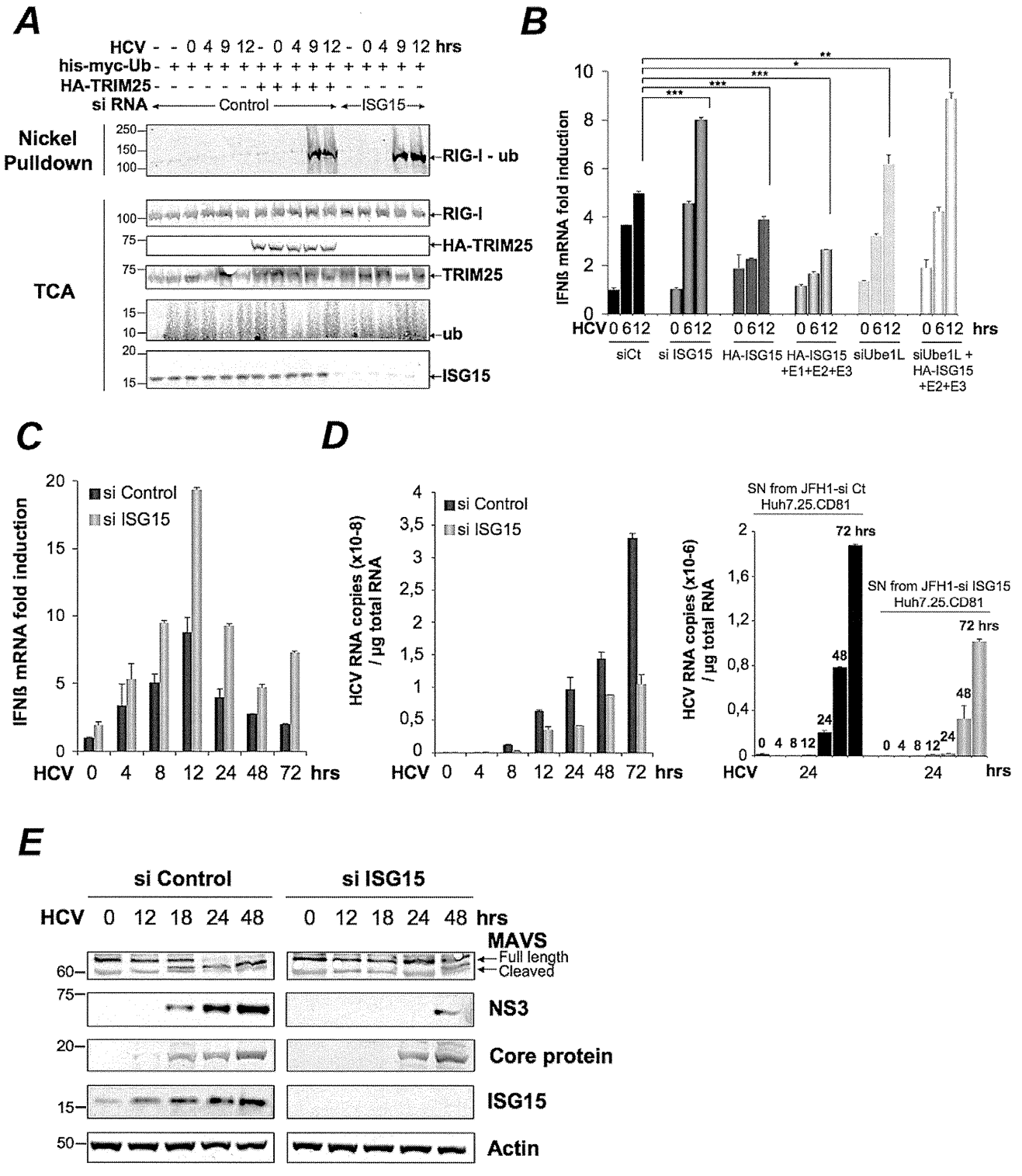

Figure 2. HCV controls RIG-I ubiquitination through ISG15. (**A**) Huh7.25.CD81 cells were transfected for 24 hrs with 25 nM of siRNA (Control or ISG15) and for another 24 hr with 5 µg of a His-Myc-Ubiquitin plasmid in absence or presence of 5 µg of a plasmid expressing HA-TRIM25. The cells were infected with JFH1 (m.o.i = 0.2). At the times indicated, cell extracts were processed for analysis of RIG-I ubiquitination and the expression of the different proteins in the total cell extracts. (**B**) Huh7.25.CD81 cells were first transfected with siRNA Control (25 nM), si RNA ISG15 (25 nM), siRNA Ube1L (50 nM) or left untreated. After 24 hrs, the untreated cells were transfected with a plasmid expressing HA-ISG15 (500 ng) alone or in presence of plasmids expressing E1, E2 and E3 (1 µg each) while a set of cells transfected with siRNA Ube1L received plasmids expressing HA-ISG15, E2 and E3. After 24 hrs, the cells were infected with JFH1 (m.o.i = 6) for the times indicated. Stimulation of endogenous IFNβ RNA expression was determined by RTqPCR and expressed as fold induction. The degree of statistical significance is indicated by stars after calculation of the p-values (from left to right: 0.0005, 0.0076, 0.0003, 0.047 and 0.0023). (**C–D**) Huh7.25.CD81 cells, transfected with 25 nM of siRNA (Control or ISG15) for 48 hrs, were infected with JFH1 (m.o.i = 6) for the times indicated. Expression of IFNβ or HCV RNA, determined by RTqPCR, was expressed as fold induction (**C**; IFNβ) or as copies (**D**; HCV). Error bars represent the mean ±S.D for triplicates. Expression levels of IFNβ RNA at the start of infection were 2.1×10^4 (siControl) and 4×10^4

copies (siISG15). Supernatants collected at different times post-infection were used to infect fresh cells. After 24 hours, the RNAs were extracted from the cells and expression of HCV RNA was determined by RTqPCR. (**E**) Huh7.25.CD81 cells, transfected with 25 nM of siRNA (Control or ISG15) for 48 hrs, were infected with JFH1 for the times indicated. Cell extracts were analysed by immunoblot with Abs directed against ISG15, MAVS, the HCV NS3 and core proteins and Actin as loading control.
doi:10.1371/journal.ppat.1002289.g002

domain (DRBD) of PKR [8], while unaffected by C16, a chemical compound which inhibits the catalytic activity of PKR (**Figure 5D**). In line with this, PRI but not C16, abrogated the ability of HCV to induce ISG15 (**Figure 5E**). The same result was obtained for induction of ISG56 (**Figure S10**). We then used human primary hepatocytes (HHP) to determine whether HCV was also able to induce ISGs through PKR in a more physiological cellular model. A follow-up of the infection over a period of 96 hours showed that JFH1 was replicating correctly in those cells as well as leading to induction of ISG15 (10-fold) and to some induction of IFNβ (2.5-fold). These cells were infected with JFH1 for 8 hours in the absence or presence of PRI, making convenient

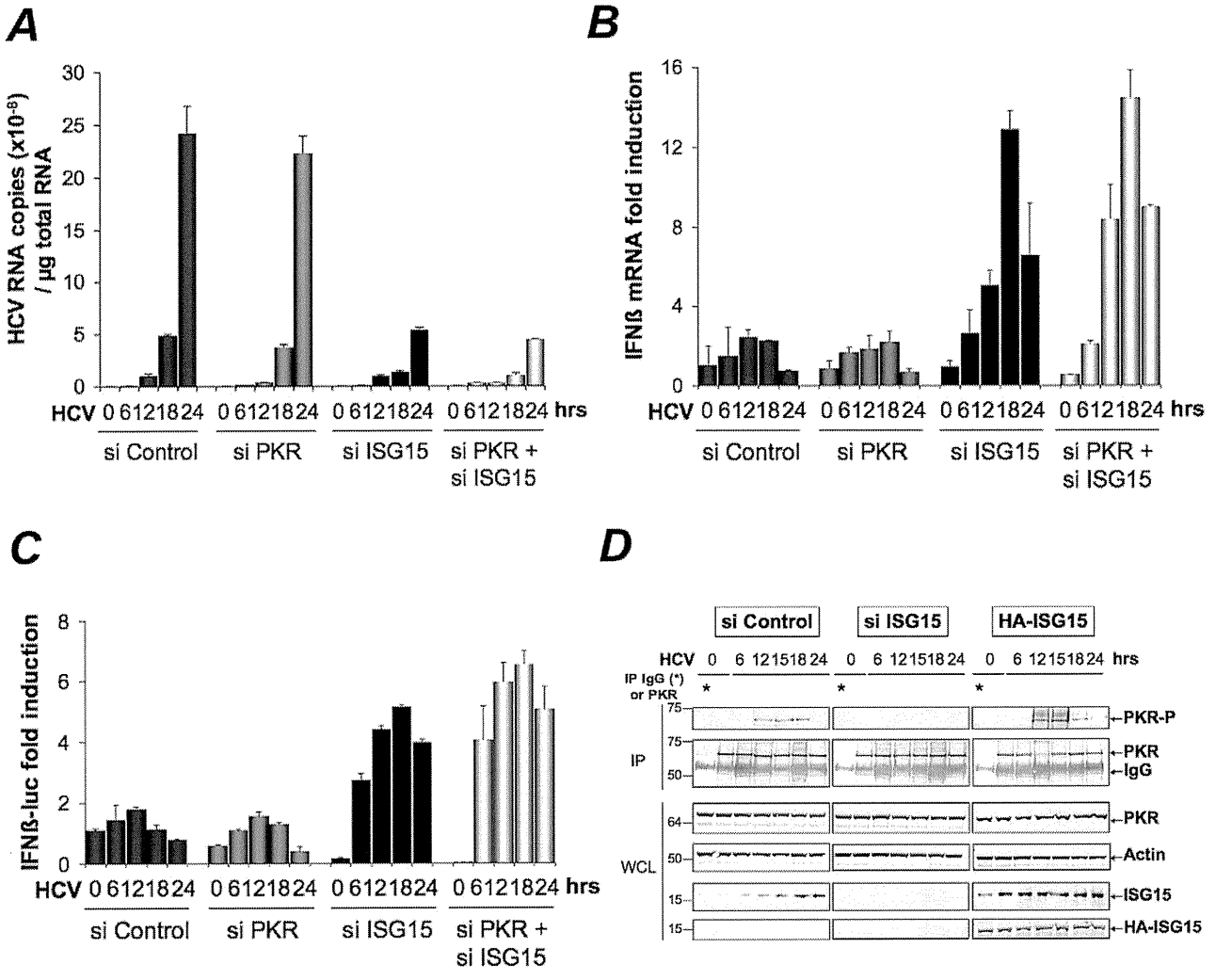

Figure 3. ISG15 strengthens the pro-HCV activity of PKR. (**A–B**). The Huh7.25.CD81 cells were transfected with 25 nM of the different siRNA (Control, ISG15, PKR), separately or together. After 48 hrs, cells were infected with JFH1 (m.o.i = 0.2). At the times indicated, expression of HCV or IFNβ RNA was determined by RTqPCR and expressed as copies of JFH1 RNA (**A**) or as fold induction (IFNβ; **B**). The expression levels of IFNβ RNA at the start of infection was 6.96×10^5 copies. (**C**) Two sets of Huh7.25.CD81 cells were first transfected with siRNA ISG15, siRNA PKR separately and together for 24 hrs, then transfected with the reporter plasmids IFNβ-firefly luciferase (pGL2-IFNβ), pRL-TK Renilla-luciferase for another 24 hrs and infected with JFH1 (m.o.i = 0.2) for the times indicated. In each case, IFN expression was expressed as fold-induction over control cells that were simply transfected with pGL2-IFNβ-FLUC/pRL-TK-RLUC. The graph represents the level of firefly luciferase activity normalized to the ratio R-luc RNA/GAPDH RNA. Such normalization is required because of the negative control of general translation through PKR after 12 hrs post-infection [8]. Error bars represent the mean ±S.D for triplicates. (**D**) Huh7.25.CD81 cells, in 100 cm^2 plates, were transfected with siRNA Control or siRNA ISG15 or transfected with a plasmid expressing HA-ISG15 for 48 hrs and infected with JFH1 (m.o.i = 6). At the indicated times post-infection, cell extracts (2.2 mg) were processed for immunoprecipitation of PKR or for incubation with mouse IgG as a control of specificity (asterisk). The immunoprecipitated complexes were run on two different NuPAGE gels and blotted using Mab 71/10 or anti-phosphorylated PKR antibodies (PKR-P). The presence of PKR and PKR-P was revealed using the Odyssey procedure. The ratio PKR-P/PKR in the absence or in the presence of ISG15, either endogenous or endogenous and ectopic, is shown in Figure S5.
doi:10.1371/journal.ppat.1002289.g003

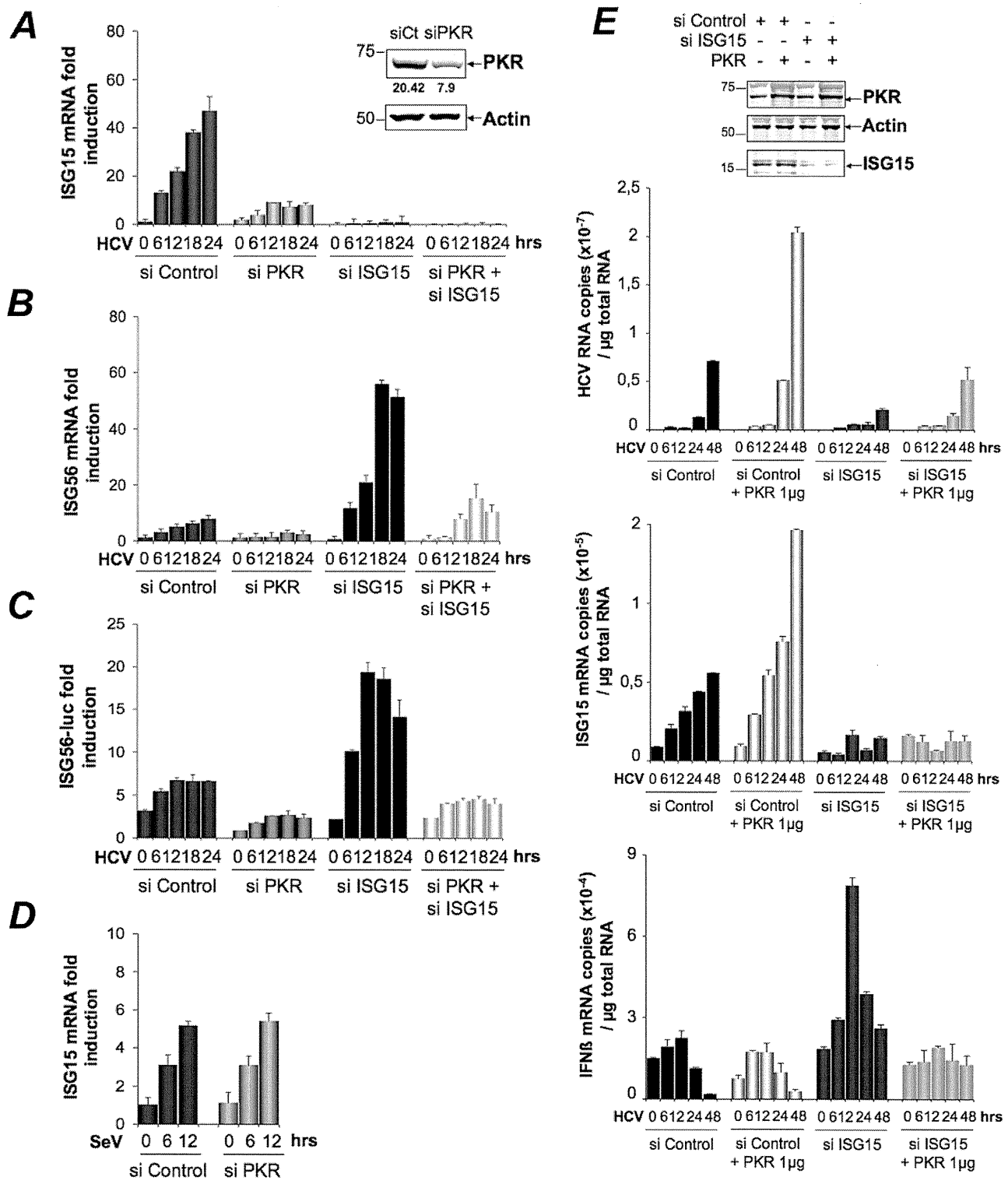

Figure 4. HCV triggers a PKR-dependent pathway early in infection to induce ISG15 and other genes. (**A–C**) The cDNAs reversed transcribed from the RNAs extracted from the Huh7.25.CD81 cells for the experiment described under Figure 3A were analysed by qPCR for the expression of ISG15 (**A**) and ISG56 (**B**). Expression levels of ISG15 and ISG56 RNA at the start of infection were respectively 1×10^5 and 1.18×10^5 copies. A novel set of Huh7.25.CD81 cells were transfected with siRNA Control, siRNA ISG15, siRNA PKR separately and together for 48 hrs. They were then transfected with the reporter plasmids ISG56-FLUC and pRL-TK-RLUC and infected with JFH1 (m.o.i = 0.2). At the times indicated, the effect of the different conditions of silencing on the reporter expression was analyzed after normalization performed as described under Figure 3C (**C**). Results are expressed as fold induction. Error bars represent the mean ±S.D for triplicates. (**D**) Huh7.25.CD81 cells were either transfected with 25 nM of siRNA Control or siPKR for 24 hrs and infected with SeV for the times indicated. Expression of endogenous ISG15 was determined by RTqPCR and expressed as fold induction. Error bars represent the mean ±S.D for triplicates. The expression levels of ISG15 RNA at the start of infection were respectively 4.91×10^4 copies (siControl) and 5.44×10^4 copies (siPKR). (**E**) Huh7.25.CD81 cells were either transfected with 25 nM of siRNA Control or

siISG15 and with 1 μg of a plasmid expressing PKR where indicated. After 48 hrs, the cells were infected with HCV (m.o.i = 6) for the times indicated. Expression of HCV, ISG15 and IFNβ RNA was determined by RTqPCR. Cell lysates prepared from cells treated in the same conditions but not infected were used to control expression of PKR and ISG15 by immunoblot.
doi:10.1371/journal.ppat.1002289.g004

use of the cell-penetrating ability of this peptide. Longer period of treatment with PRI were not investigated for practical reasons (see Materials and Methods). The results showed that PRI was significantly inhibiting the induction of ISG15 while it had no effect on that of IFNβ (**Figure 5F**). Altogether, these data demonstrate that HCV triggers induction of early ISGs through MAVS and TRAF3 by using PKR as an adapter protein.

PKR interacts both with MAVS and TRAF3 and binds HCV RNA ahead of RIG-I

The ability of HCV to control activation of the RIG-I/MAVS pathway after induction of ISG15 through a novel PKR/MAVS pathway suggests that PKR has the possibility to bind MAVS prior to RIG-I. To determine this, we established the kinetics of these interactions, after treating the Huh7.25.CD81 cells with siRNAs targeting ISG15 prior to HCV infection. This was necessary in view of the negative control of ISG15 on RIG-I. MAVS was immunoprecipitated from the cell extracts at different times post-infection and the presence of PKR and RIG-I was examined in the immunocomplexes, as well as that of TRAF3, used as marker of activation of the MAVS signaling pathway. As expected, only PKR was able to associate with MAVS and TRAF3 in the control cells (**Figure 6A**) whereas both PKR, RIG-I and TRAF3 were found in the immunocomplexes in the absence of ISG15 (**Figure 6B**). The PKR/MAVS association took place at 4 hrs post-infection in the control cells but was observed 2 hrs earlier in the ISG15-depleted cells. Whether ISG15 plays a role in the regulation of the PKR/MAVS association remains to be determined. However, the presence of TRAF3 in association with MAVS at 2 hrs post-infection in the control cells (**Figure 6A**) correlates with its association with PKR (**Figure 5C**) which indicates that the MAVS pathway can be activated through PKR as soon as 2 hrs post infection. In ISG15 knock-down cells, the RIG-I/MAVS association occurred later at 6 hrs post-infection with an increase in TRAF3 association at 9–12 hrs post infection. Altogether, these data revealed that HCV infection triggers an earlier interaction of MAVS with PKR than with RIG-I.

Finally, we asked whether PKR was able to associate with HCV RNA and how this association can be compared to that of RIG-I. PKR and RIG-I were immunoprecipitated at 2, 4 and 6 hrs post-infection and the presence of HCV RNA was analysed in the complexes. The results showed that PKR associates with HCV RNA with best efficiency at 2 hrs post-infection. Importantly, this association was strongly inhibited in presence of PRI, thus confirming the importance of PKR DRBD in the process. In contrast, the association of HCV RNA with RIG-I was detected only at 6 hrs post-infection. Interestingly, the association between RIG-I and HCV RNA was not affected by PRI, which rules out the possibility that the initial formation of a complex between PKR and HCV RNA was a pre-requisite for the subsequent binding of RIG-I to HCV RNA. Immunoprecipitation of PKR at 1, 2, 4 and 6 hrs post-infection, in presence of an inhibitor of ribonucleases also did not lead to detection of RIG-I in the complexes (**Figure S11**). Association of HCV RNA with eIF2α, used as negative control, was not significant, thus showing the specificity of the assay (**Figure 6C**). Whether a direct interaction of PKR with HCV RNA represents the initial event leading to the MAVS-dependent induction of early ISGs remains now to be characterized. Altogether, these data reveal an earlier mobilization of PKR than RIG-I in response to HCV infection which leads to activation of a MAVS-dependent signaling pathway.

Discussion

Hepatitis C virus can attenuate IFN induction at multiple levels in infected hepatocytes, such as through the NS3/4A-mediated MAVS cleavage [7,27] and by using the eIF2α kinase PKR to control IFN and ISG expression at the translational level [8,9]. Here, we have identified another process by which HCV controls IFN induction at the level of RIG-I ubiquitination through ISG15 and an ISGylation process. Importantly, we have shown that ISG15 is rapidly induced, among other ISGs, in response to HCV infection, through a novel signaling pathway that involves PKR, MAVS, TRAF3 and IRF3 but not RIG-I. In this pathway, PKR is not used for its kinase function but rather as an adapter protein with its dsRNA binding domain (DRBD) playing an essential role in this mechanism (**Figure 7**). By transcriptome analysis, we showed that HCV induces a number of ISGs in the HCV-permissive Huh7.25.CD81 cells and we confirmed the induction of two of these, ISG15 and ISG56, in other HCV-permissive cells, such as Huh7.5 and Huh7 cells. In addition, induction of ISG15 by HCV in a PKR-dependent manner was confirmed in human primary hepatocytes. The ability of HCV to trigger high expression levels of ISG15 and ISG56, as well as other ISGs, has previously been reported in models of HCV-infected chimpanzees [10,12,28] and in HCV-infected patients [14,15,16]. Induction of ISGs thus represents a general propriety of the response of the cells to HCV. In addition to this, natural variations in intra-hepatic levels of ISG15 *in vivo* may increase the susceptibility of some patients to HCV infection. The ability of HCV to control RIG-I activity through ISG15 is important to note in view of several reports which highlight the importance of a role for ISG15 in the maintenance of HCV in livers [15,16] or in the control of HCV replication in cell cultures [17,25]. Our data provide an explanation for the presence of ISGs at high expression levels in HCV-infected patients [14,15,16] and in models of HCV-infected chimpanzees [10,12,28] in the absence of, or with poor IFN expression.

The 15 Kda ISG15, or Interferon Stimulated Gene 15 [29], also known as ubiquitin cross reactive protein (UCRP) [30], can be conjugated (ISGylation) to more than 150 cellular protein targets [31] through the coordinated action of three E1, E2 and E3-conjugating enzymes, in a process similar but not identical to ubiquitination. While both ubiquitin and ISG15 can use the same E2 enzyme UbcH8, Ube1L functions as a specific E1 enzyme for ISG15, in spite of its 45% identity with Ube1, the E1 enzyme for ubiquitin [32]. The major E3 ligase for human ISG15 is HERC5 [33].

Interestingly, RIG-I was identified as a target for ISG15, among other IFN-induced proteins or proteins involved in IFN action [31]. However, its activity appears to be negatively controlled by ISG15 and the ISGylation process, either as shown previously after cotransfection with the ISG15 and the ISG15-conjugating enzymes [18] or as shown here, in a model of infection with HCV. Indeed, ISG15 is now emerging as playing a proviral role in case of HCV infection. Several reports now highlight the importance of a role for ISG15 in the control of HCV replication in cell cultures [17,25] as well as in the maintenance of HCV in livers and

Table 1. PKR-dependent up-regulated genes upon HCV infection.

SiPKR mock/siCt	Name	Access. N.	siCtMock	siCt HCV	siCtMock'	siPKRHCV	LOG2*
0,6	**ISG56**	NM_001548	15,0	885,8	10,2	7,6	-6,3
0,7	**ISG15**	NM_005101	593,6	26061,9	410,6	283,5	-6,0
0,7	**IFI 9-27/IFITM1**	NM_003641	27,8	817,7	15,1	10,1	-5,5
1,2	**IFI1-8U**	NM_006435	24,0	597,7	10,9	7,2	-5,3
1,1	Olfactory Receptor 9I1	NM_001005211	26,6	473,1	10,1	4,8	-5,2
1,6	IFI1-8U	XM_084845	17,7	365,4	9,3	6,5	-4,9
0,8	**OASp100**	NM_006187	46,4	909,9	40,0	33,5	-4,5
0,8	**IFI6-16**	NM_002038	834,5	10040,6	45,9	24,1	-4,5
0,6	**Ub2L6**	NM_004223	392,7	4078,9	281,2	128,7	-4,5
0,9	**OAS 1**	NM_016816	49,9	704,03	31,8	21,6	-4,4
0,9	**ISG12**	NM_005532	46,3	592,54	38,3	29,2	-4,1
0,8	**IFP 35**	NM_005533	36,3	369,7	26,6	16,9	-4,0
0,6	PARP-9	NM_031458	29,5	318,5	37,8	25,6	-4,0
0,5	GABA-B receptor 1	NM_006398	29,5	500,8	26,0	28,5	-4,0
0,7	**Lysp100B**	NM_003113	8,7	93	8,5	6,1	-3,9
0,8	PDIP1	NM_033405	27,4	146,6	28,0	12,8	-3,6
0,8	**PKR**	NM_002759	48,2	306,8	47,0	26,0	-3,5
1,6	**MT-IM**	NM_176870	49,0	1371,8	6,9	19,6	-3,3
0,7	**Phospholipid scramblase**	NM_021105	170	1137,2	189,9	153	-3,1
1,1	**RIG-I**	NM_014314	23,5	223,2	18,9	21,9	-3,0
0,6	**IFIT-5**	NM_012420	24,9	95,3	35,0	21,3	-2,7
1,3	RIG-I	NM_004585	7,4	42,5	6,3	6,0	-2,6
0,7	**STAT1 beta**	NM_139266	336,9	1401,5	300,3	210,3	-2,6
0,8	BRCA1 C-ter assoc. Prot	NM_001040444	12,3	45,1	8,1	5,1	-2,6
0,9	Cohesin Rec8 homolog	NM_005132	18,0	103	16,7	16,9	-2,5
0,5	C/EBPdelta	NM_005195	324,9	901,8	278,9	161,27	-2,3
0,7	ZNF532	NM_018181	32,8	146,5	25,5	23,8	-2,3
0,6	NNMT	NM_006169	52,8	143,8	50,26	28,9	-2,2
1	ISG1-8U	XM_084845	32,0	146,8	23,1	22,7	-2,2
1,1	HIF00	NM_153833	45,3	199,9	34,7	32,9	-2,2
0,8	**ISG20**	NM_002201	129,3	338,3	107,5	61,4	-2,2
1,1	PSMB10	NM_002801	16,2	75,1	14,5	15,0	-2,2
1,3	ZC3HAV1	NM_024625	8,3	26,0	6,9	4,9	-2,1
0,9	SOD2	NM_000636	348,5	1612,2	311	334,3	-2,1
0,7	PARP12	NM_022750	269,9	875,2	296,9	224,2	-2,1
0,7	NMI	NM_004688	32,1	136	37,4	37,0	-2,1
0,8	NEDD9	NM_006403	5,7	19,0	5,7	4,7	-2,0
1,1	**SAMHD1**	NM_015474	17,1	49,5	13,6	9,7	-2,0
0,7	AKT2	NM_001626	13,4	20,0	14,2	5,4	-2,0
0,5	ARG1	NM_000045	245,9	282,6	231,4	67,0	-2,0
0,8	BHLHB2	NM_003670	76,4	128,0	71,5	30,5	-2,0
0,8	LGALS3BP	NM_005567	22,0	72,0	16,1	13,6	-2,0
1,3	ZNF292	XM_048070	22,3	31,4	20,2	7,3	-2,0
1,1	STAT1	NM_007315	53,3	275,3	48,2	64,9	-1,9
0,7	TBA3_HUMAN	NM_006009	28,2	43,6	33,4	13,7	-1,9
0,5	TM4SF20	NM_024795	45,2	51,0	36,9	11,1	-1,9
1,4	ERAP2	NM_022350	9,8	19,2	8,8	4,6	-1,9
0,8	**USP18**	XM_001126794.1	215,1	979,2	201,8	245,9	-1,9
1	USP18	XM_001126794.1	129,6	617,0	127,3	165,5	-1,9